


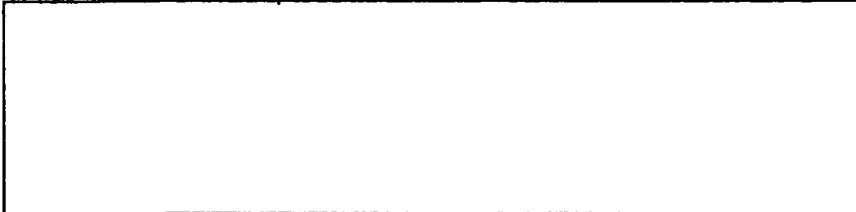
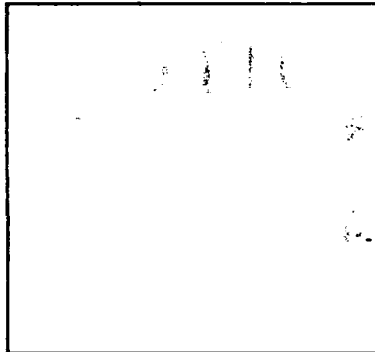
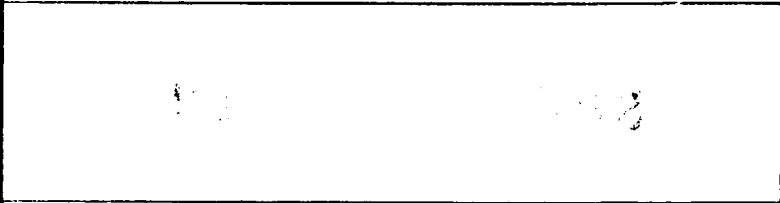
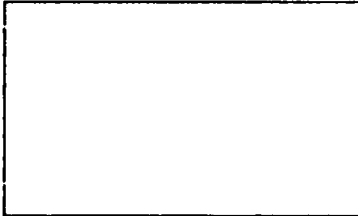
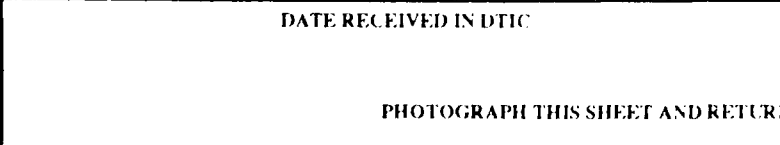
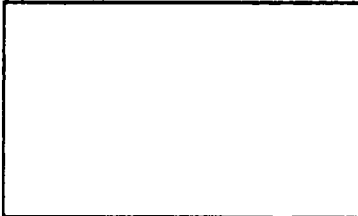


LOAN DOCUMENT

AD-A238 483 	DTIC ACCESSION NUMBER		PHOTOGRAPH THIS SHEET																												
		LEVEL		INVEN																											
		<u>WL-TR-91-4048</u> DOCUMENT IDENTIFICATION <u>May 1991</u>																													
																															
		DISTRIBUTION STATEMENT																													
<table border="1"><tr><td colspan="2">ACCESSION FOR</td></tr><tr><td>NTIS</td><td>GRA&I <input checked="" type="checkbox"/></td></tr><tr><td>DTIC</td><td>TRAC <input type="checkbox"/></td></tr><tr><td>UNANNOUNCED</td><td><input type="checkbox"/></td></tr><tr><td>JUSTIFICATION</td><td></td></tr><tr><td colspan="2"> </td></tr><tr><td colspan="2"> </td></tr><tr><td colspan="2"> </td></tr><tr><td colspan="2">BY</td></tr><tr><td colspan="2">DISTRIBUTION/</td></tr><tr><td colspan="2">AVAILABILITY CODES</td></tr><tr><td>DISTRIBUTION</td><td>AVAILABILITY AND/OR SPECIAL</td></tr><tr><td rowspan="2">A-1</td><td></td></tr><tr><td></td></tr></table>		ACCESSION FOR		NTIS	GRA&I <input checked="" type="checkbox"/>	DTIC	TRAC <input type="checkbox"/>	UNANNOUNCED	<input type="checkbox"/>	JUSTIFICATION								BY		DISTRIBUTION/		AVAILABILITY CODES		DISTRIBUTION	AVAILABILITY AND/OR SPECIAL	A-1					
ACCESSION FOR																															
NTIS	GRA&I <input checked="" type="checkbox"/>																														
DTIC	TRAC <input type="checkbox"/>																														
UNANNOUNCED	<input type="checkbox"/>																														
JUSTIFICATION																															
BY																															
DISTRIBUTION/																															
AVAILABILITY CODES																															
DISTRIBUTION	AVAILABILITY AND/OR SPECIAL																														
A-1																															
DISTRIBUTION STAMP		DATE ACCESSIONED																													
																															
DATE RECEIVED IN DTIC		DATE RETURNED																													
																															
		REGISTERED OR CERTIFIED																													

PHOTOGRAPH THIS SHEET AND RETURN TO DTIC-FDAC



AD-A238 483



COUNTERDOPED HIGH TEMPERATURE, SILICON
ARRAY INFRARED DETECTOR

John A. Baker

Universal Energy Systems, Inc.
4401 Dayton-Xenia Road
Dayton, Ohio 45432

May 1991

Final Report for Period April 1986 - April 1987

Approved for public release; distribution is unlimited.

MATERIALS DIRECTORATE
WRIGHT LABORATORY
AIR FORCE SYSTEMS COMMAND
WRIGHT-PATTERSON AIR FORCE BASE, OHIO 45433-6533

NOTICE

When Government drawings, specifications, or other data are used any purpose other than in connection with a definitely Government-rel procurement, the United States Government incurs no responsibility or obligation whatsoever. The fact that the government may have formulate in any way supplied the said drawings, specifications, or other data, is to be regarded by implication, or otherwise in any manner construed, licensing the holder, or any other person or corporation; or as convey any rights or permission to manufacture, use, or sell any patented invention that may in any way be related thereto.

This report is releasable to the National Technical Information Service (NTIS). At NTIS, it will be available to the general public, including foreign nations.

This technical report has been reviewed and is approved for publication.

Gail J. Brown
GAIL J. BROWN, Project Monitor
Electronic & Optical Materials Br.
Electromagnetic Mat'ls & Surv. Div.

Lyle G. Riffie
LYLE G. RIFFEE, Actg. Chief
Electronic & Optical Materials
Electromagnetic Mat'ls & Surv. Div.

FOR THE COMMANDER:

William R. Woody
WILLIAM R. WOODY, Chief
Electromagnetic Mat'ls & Surv. Div.
Materials Directorate
Wright Laboratory

If your address has changed, if you wish to be removed from our mailing list, or if the addressee is no longer employed by your organization please notify WL/MLPO, WPAFB, OH 45433-6533 to help us maintain a current mailing list.

Copies of this report should not be returned unless return is required for security considerations, contractual obligations, or notice on a specific document.

Unclassified

SECURITY CLASSIFICATION OF THIS PAGE

REPORT DOCUMENTATION PAGE				For ON
1a. REPORT SECURITY CLASSIFICATION Unclassified			1b. RESTRICTIVE MARKINGS	
2a. SECURITY CLASSIFICATION AUTHORITY			3. DISTRIBUTION / AVAILABILITY OF REPORT Approved for Public Release; Distribution is Unlimited	
2b. DECLASSIFICATION / DOWNGRADING SCHEDULE				
4. PERFORMING ORGANIZATION REPORT NUMBER(S)			5. MONITORING ORGANIZATION REPORT NUMBER WL-IR-91-4048	
6a. NAME OF PERFORMING ORGANIZATION Universal Energy Systems, Inc.		6b. OFFICE SYMBOL (If applicable)	7a. NAME OF MONITORING ORGANIZATION Materials Directorate (WL/ML) Wright Laboratory	
6c. ADDRESS (City, State, and ZIP Code) 4401 Dayton-Xenia Rd Dayton OH 45432			7b. ADDRESS (City, State, and ZIP Code) Wright-Patterson AFB OH 4543	
8a. NAME OF FUNDING / SPONSORING ORGANIZATION Materials Directorate		8b. OFFICE SYMBOL (If applicable) WL/MLPU	9. PROCUREMENT INSTRUMENT IDENTIFICATION NUMBER F33615-86-C-5091	
8c. ADDRESS (City, State, and ZIP Code) Wright Laboratory Wright-Patterson AFB OH 45433-6533			10. SOURCE OF FUNDING NUMBERS	
			PROGRAM ELEMENT NO 65502F	PROJECT NO 3005
11. TITLE (Include Security Classification) Counterdoped High temperature, Silicon Array Infrared Detector				
12. PERSONAL AUTHOR(S) Baker, John A.				
13a. TYPE OF REPORT Final Report		13b. TIME COVERED FROM 4/86 TO 4/87	14. DATE OF REPORT (Year, Month, Day) May 1991	15. PAGE 8
16. SUPPLEMENTARY NOTATION				
17. COSATI CODES			18. SUBJECT TERMS (Continue on reverse if necessary and identify by block number) Counterdoping, silicon, electron irradiation, detector, extrinsic	
FIELD	GROUP	SUB-GROUP		
17	05			
19. ABSTRACT (Continue on reverse if necessary and identify by block number) A counterdoped infrared detector system consisting of a silicon substrate doped and divacancies has been created. High purity polycrystalline silicon was further purified by float zoning to reduce impurity levels still present; it was then back doped with boron. Electron irradiation was used to create the divacancies which become the active infrared centers. Boron compensates the newly created divacancies thus producing only positively charged divacancies. These positively charged divacancies are stable under illumination. The experimental results thus verify the theoretical model postulated by Elliott for counterdoping. A theoretical analysis of multivalent statistics as applied to counterdoped detectors developed an extended model for counterdoped detectors. This model has identified relevant parameters which control the operating temperature and figure of merit.				
20. DISTRIBUTION / AVAILABILITY OF ABSTRACT <input type="checkbox"/> UNCLASSIFIED/UNLIMITED <input type="checkbox"/> SAME AS RPT <input checked="" type="checkbox"/> DTIC USERS			21. ABSTRACT SECURITY CLASSIFICATION Unclassified	
22a. NAME OF RESPONSIBLE INDIVIDUAL Gail J. Brown			22b. TELEPHONE (Include Area Code) (513) 255-4474	22c. OFFICE WL/ML

Block 19.

counterdoped detector. The model may be used to optimize doping concentration for highest background limited infrared photoconductor (BLIP) operating temperature.

TABLE OF CONTENTS

<u>SECTION</u>	<u>PAGE</u>
1.0 INTRODUCTION	1
1.1 GENERAL CONCEPT OF COUNTERDOPED DETECTORS	1
1.2 BORON-DIVACANCY COUNTERDOPED SYSTEM	1
1.3 PHASE I OBJECTIVES	3
1.4 DIVACANCY PRODUCTION	5
2.0 EXPERIMENTAL PROCEDURES	6
2.1 FLOAT ZONE OPERATION: BORON DOPING	6
2.2 DEEP LEVEL TRANSIENT SPECTROSCOPY (DLTS)	7
2.3 THE HALL EFFECT	12
3.0 EXPERIMENTAL DATA	13
3.1 DLTS UNIT NO. 1	13
3.1.1 C-V AND DLTS ANALYSIS	13
3.1.2 DLTS EQUIPMENT	14
3.1.3 EXPERIMENTAL RESULTS	14
3.2 DLTS UNIT NO. 2	17
3.3 HALL ANALYSIS	24
3.4 INFRARED ANALYSIS	28
4.0 APPLICATION OF MULTIVALENT STATISTICS TO COUNTERDOPED DETECTORS	34
4.1 INTRODUCTION	34
4.2 THE DIVACANCY	34
4.3 MULTIVALENT STATISTICS	35
4.4 CHARGE BALANCE FOR THE DIVACANCY	37
4.5 DEGENERACY	38
4.6 RATE EQUATIONS	42
4.7 DETECTOR RESPONSE	45
4.8 THERMAL EQUILIBRIUM, HIGH BORON CASE	51
4.9 BACKGROUND ILLUMINATED CASE	53
4.9.1. Low Boron, with Illumination	54
4.9.2. High Boron, with Illumination	58
4.10 RESPONSIVITY	60
4.11 DETECTIVITY	62
5.0 CONCLUSION	65
ACKNOWLEDGEMENTS	66
REFERENCES	67
APPENDIX	69

LIST OF FIGURES

<u>FIGURE</u>		<u>PAGE</u>
1-1	DOUBLE IONIZED DONOR	2
1-2	DOUBLE IONIZED ACCEPTOR	2
1-3	BORON-DIVACANCY COUNTERDOPED BLIP SYSTEM	4
2-1	ISOTHERMAL CAPACITANCE TRANSIENT	8
2-2	RATE WINDOW CONCEPT	9
2-3	TRANSIENT AMPLITUDE	11
3-1-1	$1/C^2$ VS. V	15
3-1-2	EQUIPMENT BLOCK DIAGRAM	16
3-1-3	ARRHENIUS PLOT 1	18
3-1-4	PEAK IDENTIFICATION	19
3-2-1	TWO LOW TEMPERATURE DEFECTS	21
3-2-2	THERMAL ACTIVATION ENERGY	22
3-2-3	PEAK HEIGHT VS. TEMPERATURE	23
3-3-1	HOLE CONCENTRATION VS. $1000/T$	26
3-3-2	CALCULATED FIT	27
3-3-3	CALCULATED FIT $E_{A3} = 0.21\text{eV}$	29
3-4-1	BORON SPECTRA (5K)	31
3-4-2	$V_{\frac{1}{2}}$ SPECTRA (5K)	32
4-1	LEVELS OF DIVACANCY IN SILICON	39
4-2	ELECTRON OCCUPANCY OF THE DANGLING BOND STATES OF THE DIVACANCY AND THE DIVACANCY AND THE ASSOCIATED DEGENERACY FACTORS	41
4-3	CHARGE CENTER CONCENTRATIONS $\phi_B = 0$ $N_B = 5 \times 10^{12}$	48
4-4	CHARGE CENTER CONCENTRATIONS $N_B = N_D$	52
4-5	LOW COUNTERDOPED SYSTEMS	55
4-6	HIGH COUNTERDOPED SYSTEMS	56
4-7	CALCULATED RESPONSIVITY	61
4-8	DETECTIVITY VS. TEMPERATURE	64

LIST OF TABLES

<u>TABLE</u>	<u>PAGE</u>
1-1 IMPURITY CONTENT IN SILICON	6
4-1 INPUT PARAMETERS FOR THE CALCULATION OF THE DETECTOR RESPONSE	46

1.0 INTRODUCTION

1.1 GENERAL CONCEPT OF COUNTERDOPED DETECTORS

The development of a counterdoped infrared detector is due to Elliott.^[1-1] A background limited infrared photoconductor (BLIP) which operates at high temperature (80K) is made possible using the technique described by Elliott et al. A normal infrared detector will exhibit a very large capture cross-section of an ionized acceptor for a hole. This large capture cross-section (attraction of carriers and photoionized centers) leads to short carrier lifetimes which result in low operating temperatures for the detector. The counterdoped system shows that holes are captured by donors which are neutral or positively charged; the capture cross-section in this case is very small because the photoionized center is neutralized in the photoabsorption. This resulting lower recombination cross-section increases the carrier lifetime permitting development of a BLIP detector which will operate at high temperature (80K or higher).

The counterdoping technique calls for doping a semiconductor with either a deep donor (Figure 1-1) or a deep acceptor (Figure 1-2) and then counterdoping the semiconductor with a shallow impurity of the opposite kind. The infrared detector thus constructed consists of an infrared active center (the deep impurity [donor or acceptor]) which has lost charge to the compensating counterdopant. The deep acceptor is now negatively charged for the deep acceptor - shallow donor case. The deep donor is positively charged if we have the deep donor - shallow acceptor case.

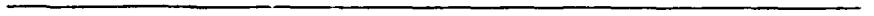
1.2 BORON-DIVACANCY COUNTERDOPED SYSTEM

We have chosen the shallow acceptor (0.045eV) (Boron) - deep donor (0.20eV, 0.73eV, 0.9eV) (Divacancy) system to construct a counterdoped infrared detector. The principal infrared active dopant is the deep donor. The concentration of boron was chosen to be of the order of 1×10^{17} atoms/cm³; to permit the deep donor to be the active element, w

E_C



E_{T^+}



$E_{T^{++}}$



E_F



E_A



E_V

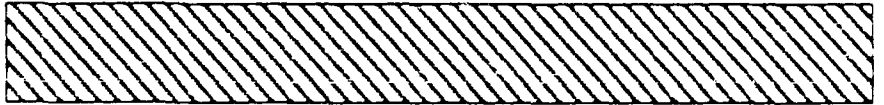


Figure 1-1 Double Ionized Donor

E_C



E_D



E_F



$E_{T^{--}}$



E_{T^-}



E_V



Figure 1-2 Double Ionized Acceptor

must have the divacancy content be of the same order of concentration. It is desirable to have the number of divacancies be equal to or slightly greater than the number of boron atoms.

The schematic band diagram for this case is presented in Figure 1-3. We assumed for this case that the divacancy is either neutral or singly positively charged.

$$N_D^+ = N_A = N_A^- \text{ for } N_D \geq N_A \quad (1-1)$$

Photoconductivity occurs when we have photoabsorption of a photon, having energy greater than E_g , by a valence electron. The donor level is now neutralized by this electron and a hole is created in the valence band. The holes constitute the photocurrent; their lifetimes will be long because the recombination capture cross-section of holes by neutral donors is very small. Thus the operating temperature of the system will be higher than would be the case for a large recombination capture cross-section detector.

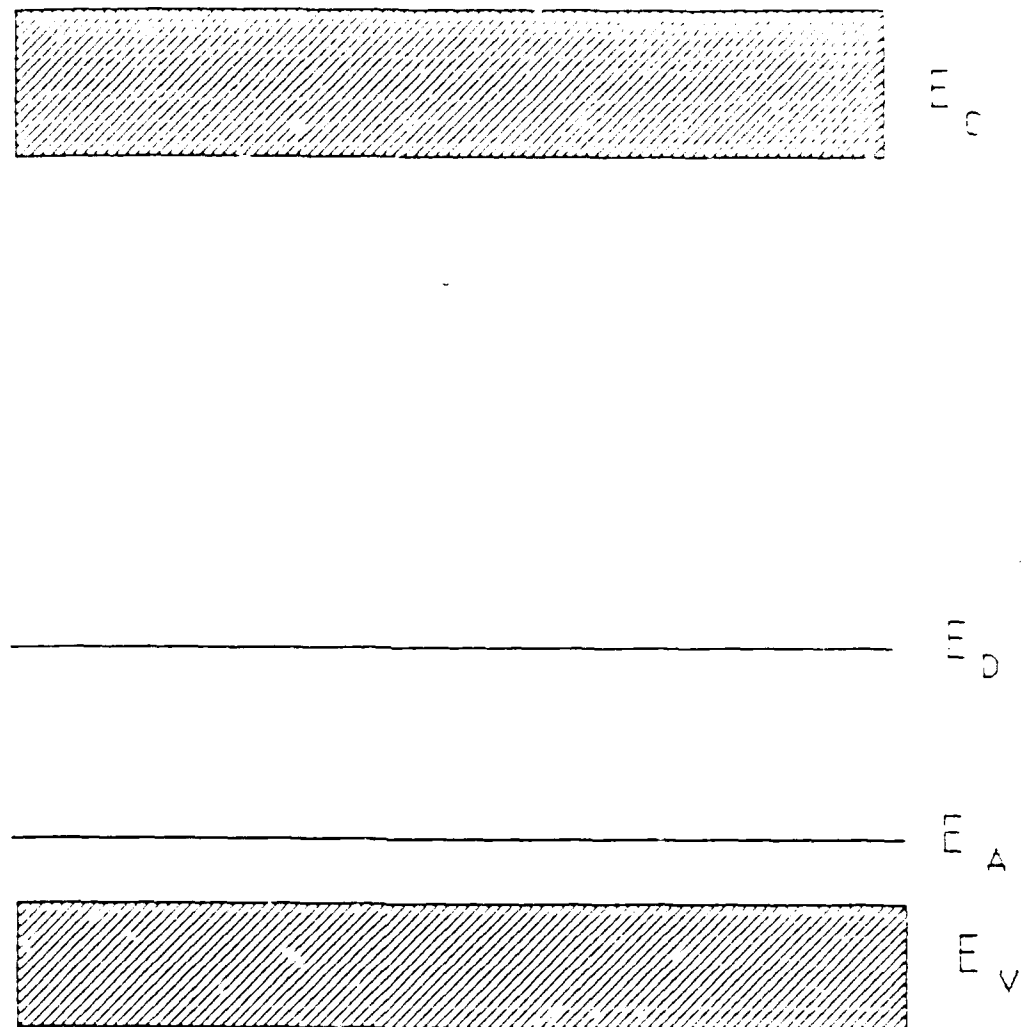
1.3 PHASE I OBJECTIVES

The performance of our Phase I activities will be evaluated against the Phase I technical objectives provided in our Phase I proposal. We insert Section 4.0 from the proposal at this position. When we discuss the experimental and theoretical results, reference will be made back to this section.

PHASE I TECHNICAL OBJECTIVES

An experimental and theoretical analysis of the Boron-Divacancy counterdoped infrared detector complex will be undertaken in this Phase I research effort.

1. Produce an identification of the variables which influence the BLIP operating temperature for the Boron-Divacancy counterdoped detector.



- E_C Conduction Band
- E_D Donor Level (Divacancy)
- E_A Acceptor Level (Boron)
- E_V Valence Band

Figure 1-3 Boron-Divacancy Counterdoped Blip System

2. Define the proper annealing procedures and temperature to maintain the high concentration of divacancies produced by electron beam irradiation.
3. Characterize the levels introduced by electron beam irradiation. Identify crystalline damage defects.
4. Define conditions for highest photoconductive response.
5. Develop theoretical model for the rate equations to predict proper doping concentrations to achieve highest BLIP operating temperature.

1.4 DIVACANCY PRODUCTION

The 2MeV electrons supply sufficient energy to create lattice vacancies in silicon on a uniform basis in depth. The threshold energy for displacement of a silicon atom from the lattice site is of the order of 30.0eV.^[1-2] First, four bonds are broken [$E = 4 \text{ times (Bond Energy) } = 23.6\text{eV}$]. Then the atom goes into an interstitial position requiring 6.5eV to push the neighboring atoms out of its path; it is necessary to surmount the barrier set up by these atoms. Finally, all the atoms relax about the vacancy. Irradiation was performed at room temperature where the lattice vacancy is mobile. This provides the longer term creation of divacancies. It is necessary to permit a stable state to set in for the creation of divacancies because the direct creation of divacancies from 2MeV electron irradiation is only about 5% that of the creation of vacancies.^[1-3]

The rule of thumb to use in direct creation of divacancies from electron irradiation is to state that 10^{-2} divacancies are created per electron.

2.0 EXPERIMENTAL PROCEDURES

2.1 FLOAT ZONE OPERATION: BORON DOPING

A Siemens VZA3 vacuum float zoner was employed to purify the polycrystalline silicon. Four zone purification passes were made. The boron was added on a fifth pass to back dope to a boron concentration of $1 \text{ E } 17 \text{ atoms/cm}^3$.

Each zone pass of the coil over the polycrystalline rod removes impurities based on a factor termed the distribution coefficient (κ).

$$C = C_0 [1 - (1 - \kappa) \exp(-\kappa x / l)] \quad (2-1)$$

where C = Concentration of element in zoned rod
 C_0 = Initial concentration of impurity element before pass
 κ = Distribution coefficient
 l = Width of molten zone
 x = Distance from seed end of crystal

Care was taken in removing impurities from the silicon rod because we did not want to have contribution to our experimental data from sources other than boron and the divacancy. The level of some major impurities is presented in Table 1-1 for our samples.

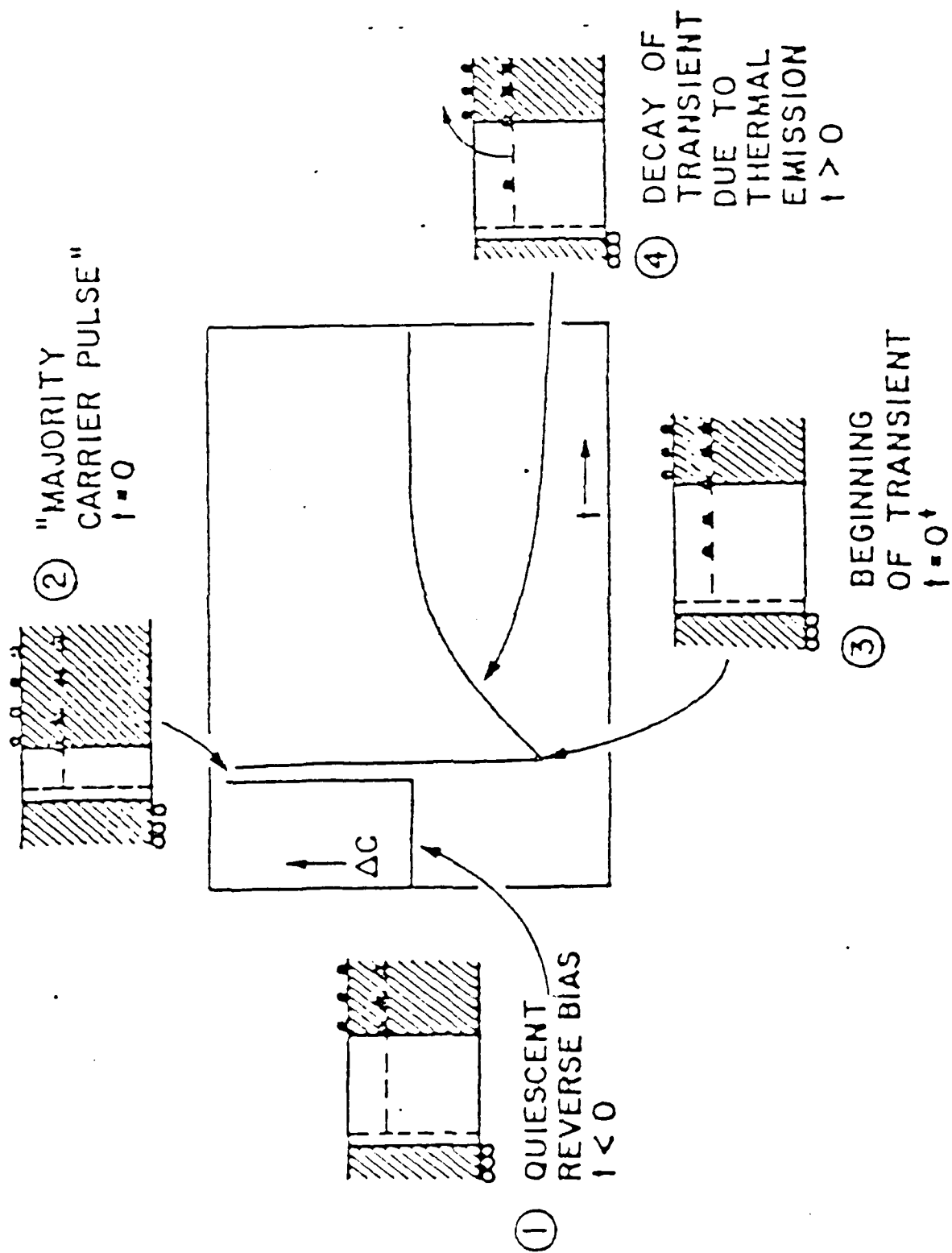
TABLE 1-1. IMPURITY CONTENT IN SILICON

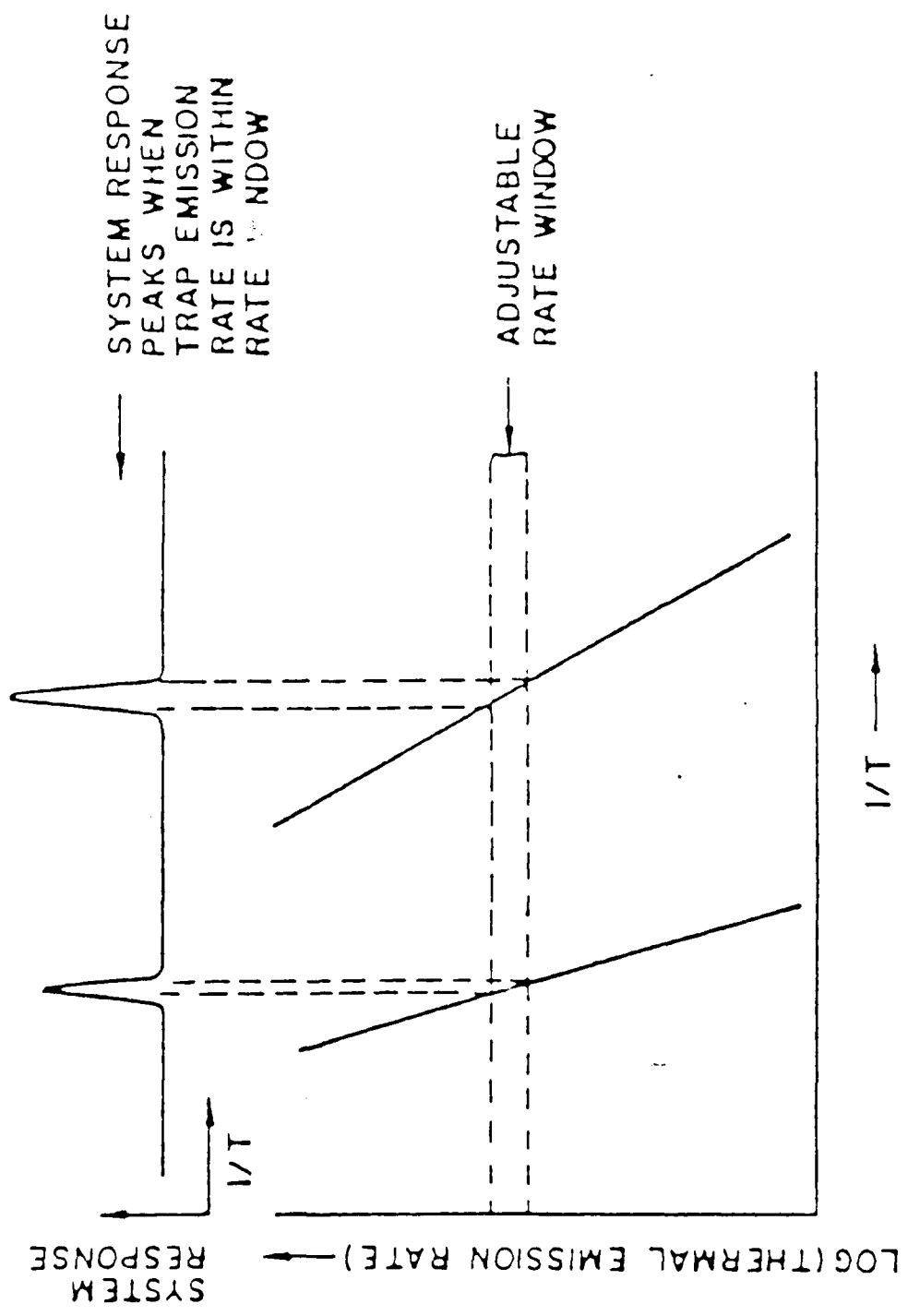
Element	Polysilicon Concentration (atoms/cm ³)	Final Single Crystal Concentration (atoms/cm ³)
Boron	$2.6 \text{ E } 12$	$1 \text{ E } 17$
Other Group III, V	$5 \text{ E } 12$	$5 \text{ E } 11$
Carbon	$5 \text{ E } 16$	$5 \text{ E } 15$
Metals	$5 \text{ E } 16$	$1 \text{ E } 13$

2.2 DEEP-LEVEL TRANSIENT SPECTROSCOPY (DLTS)

Deep-Level Transient Spectroscopy^[2-1] (DLTS), which utilizes voltage modulation of the depletion width of a semiconductor junction to detect electronic transitions at defect states located in the gap, has become, during the past ten years, the most widely used technique for microscopic identification of electronic defects in semiconductors. DLTS exploits nonradiative transitions between localized electronic states (deep levels) and band states in semiconductors, and it therefore measures thermal transition energies which may determine operational behavior of semiconductor devices. The DLTS is the most sensitive technique to detect electrically active defects and provides unique "signatures" of deep levels. DLTS and related junction spectroscopy techniques are becoming standard methods for semiconductor material characterization, processing steps monitoring and device performance evaluation.

The essential physics of DLTS is based on the effects of trapping and emission of carriers at deep energy levels which are located in the space-charge layer of a pn junction or Schottky barrier. First, we consider the thermal-emission transient at some fixed temperature. Figure 2-1^[2-2] shows a capacitance transient due to majority-carrier emission with insets describing the condition of the space-charge layer during the various phases of the transient. A capacitance change is caused by a short bias pulse which introduces carriers and thus changes the electron occupation of a deep level from its steady-state value. As this population returns to equilibrium, the capacitance returns to its equilibrium value. If we now consider a train of periodical filling pulses applied on the reverse biased junction, we then have a signal which consists of a series of transients with a constant repetition rate. As the temperature is varied, the time constant of the transient varies exponentially with $1/T$. This is shown in Figure 2-2 which illustrates the basic idea of the DLTS, the so-called rate-window concept. Thus, the DLTS analysis is a filtering operation and there are a number of ways in which the DLTS rate-window concept may be implemented in practice and a DLTS spectrum produced. The first method proposed





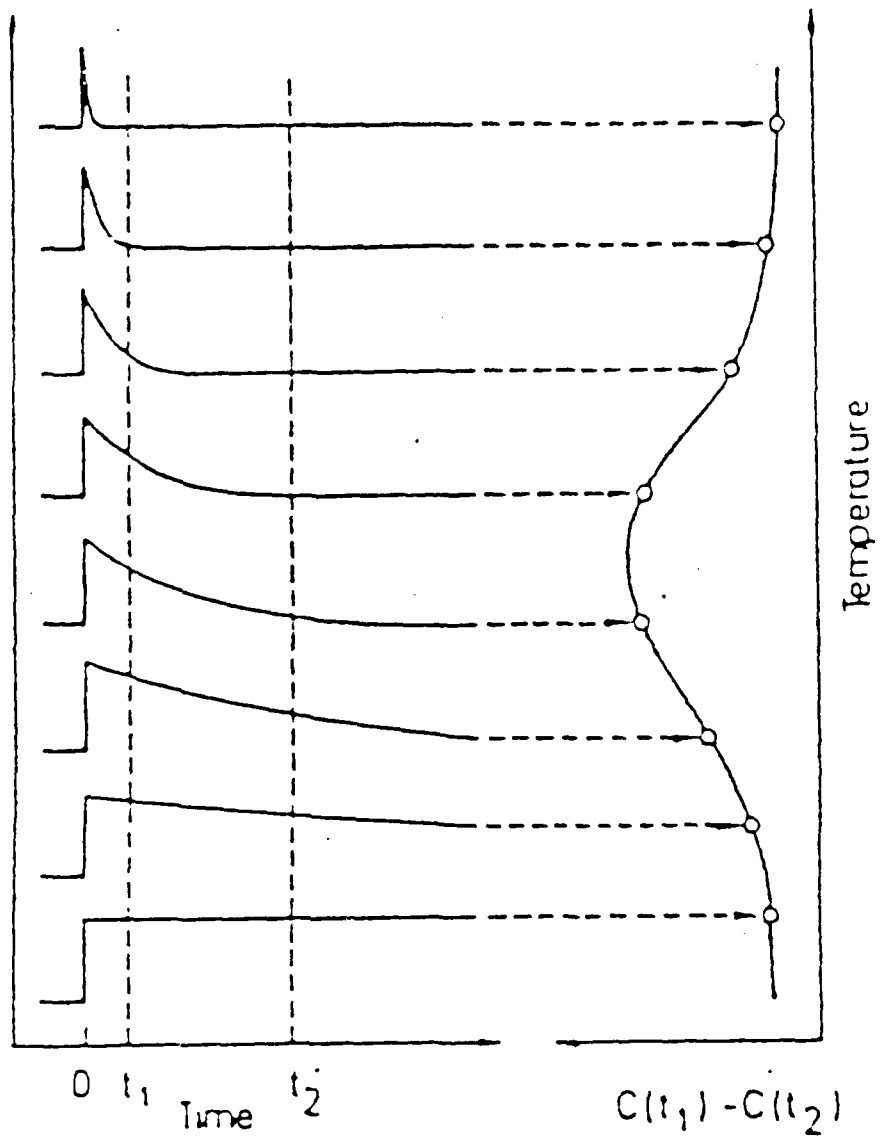
the original DLTS experiments by D.V. Lang^[2-1] was based on the use of a double-boxcar integrator. The DLTS signal is the difference between the transient amplitude at two times t_1 and t_2 , after the pulse, shown in Figure 2-3. There is zero difference at these two gates and consequently no DLTS signal for either low or high temperatures corresponding to very slow or very fast transients, respectively. A DLTS peak is generated when the transient-time constant τ is on the order of the gate separation. The rate window can be expressed in terms of the transient-time constant τ_{\max} giving rise to the maximum boxcar output as a function of temperature^[2-1], namely,

$$\tau_{\max} = \frac{t_1 - t_2}{\ln(t_1/t_2)} \quad (2-2)$$

The DLTS scan is reversible and does not depend on the magnitude of the heating or cooling rate. In general, the DLTS method can be applied to any thermally stimulated process which allows for its generation by pulsed excitation.^[2-3] The DLTS method is spectroscopic in the sense that the various DLTS peak heights are directly proportional to the respective concentration of individual defects. The spectroscopic character of DLTS allows for quantitative analysis of electrically active defects with a sensitivity of the order 10^{-5} of the shallow-level doping $[N_D - N_A]$, e.g., 10^9 cm^{-3} defects if $|N_D - N_A| = 10^{14} \text{ cm}^{-3}$. The DLTS technique, when applied to lightly doped material, is thus the most sensitive technique to detect electrically active defects.

The activation energy of a deep level can be determined in the standard manner from the slope of an Arrhenius plot. An Arrhenius plot is constructed from data obtained by recording several DLTS spectra using different rate windows and by plotting the log of the rate window from Reference 2-1 versus the inverse temperature of the DLTS peak T^{-1} . The relationship of the measured activation energy to the true depth of the deep level is complex. This is due to the temperature dependence of the capture cross-sections and due to the temperature dependence of the deep-level energy itself.^[2-3]

Capacitance transients at various temperatures



Carrier capture measurements can be done by recording the variation of peak height as a function of pulse width. The occurrence of temperature-dependent capture cross-sections must be taken into account in order to obtain the true depth of the level.^[2-3]

2.3 THE HALL EFFECT

The concentration and identity of electrically active impurities in silicon may be measured using the Hall effect. The Hall effect measurement is performed by passing a current I through a sample which has a magnetic field H applied perpendicular to I . The Hall voltage V_H is measured perpendicular to both I and H .

Initially, the magnetic field is turned off; for $H = 0$ we find that $V_H = 0$. When the magnetic field is turned on, the moving charges, represented by the applied current, are deflected by the Lorentz force in a direction perpendicular to both I and H . At steady state, the electrostatic field which is set up is termed the Hall field.

The Hall coefficient, R_H , is a function of the Hall voltage, the current, the magnetic field, and the thickness τ of the sample.

$$R_H = (V_H/I) (T/H) \quad (2-3)$$

The resistivity of the sample is calculated from knowledge of the thickness τ , the width w , and the separation of the voltage contacts l .

$$\rho = (V/I) (w\tau/l) \quad (2-4)$$

3.0 EXPERIMENTAL DATA

The DLTS spectra exhibit the various defects which are created by the electron irradiation. We see in Table 1-1 the elements of interest which may be involved in creating defect center complexes. The boron concentration of $1 \times 10^{17}/\text{cm}^3$ is so high that it is likely to see boron as a component of a number of complexes. A concentration of $5 \times 10^{15}/\text{cm}^3$ for carbon in silicon is observed as a best value for any oil pumped float zoned silicon. This level of impurity content is sufficiently high to produce an observable center. The normally expected vacancy, interstitials and divacancy defects will appear in addition to (Boron-Vacancy), boron interstitial and carbon interstitial.

We performed the electron irradiation at 300K; the vacancy defect is mobile at this temperature and will form either divacancies, B_S-V , or other complexes. We do not expect the DLTS to observe the vacancy defect by itself.

3.1 DLTS UNIT NO. 1

3.1.1 C-V and DLTS Analysis

Capacitance-Voltage (C-V) measurements were used to determine the background doping and Schottky barrier height of the samples. The barrier height measurement gives an indication of the quality of the diode. On p-type material, an Al Schottky diode would usually give a barrier height of about $1/3 V_{\text{gap}}$ or for silicon, 0.34eV. The barrier height is calculated from the slope of the $1/C^2$ vs. V curve for the diodes fabricated for this experiment ϕ_B was calculated to be 0.16eV. This low value probably indicated a reaction of the Al with the surface or the presence of surface states.

The net doping concentration calculated from the C-V data was $3.8 \times 10^{16} \text{ cm}^{-3}$ which corresponds well with the value of $2.4 \times 10^{16} \text{ cm}^{-3}$ calculated from Hall effect analysis. C-V data are usually higher due to r-factor corrections to the Hall data. This net

doping concentration is used to calculate the trap concentrations in DLTS.

The C-V data were taken on a Hewlett-Packard 4280A, 1MHz, C-V meter under control of an LSI-11/23 computer for on-line data acquisition. The $1/C^2$ vs. V curve is plotted in Figure 3-1-1.

3.1.2 DLTS Equipment

The DLTS system is a fully automated system consisting of an LSI-11/23 computer with a 30Mb Winchester disk drive. The system is shown schematically in Figure 3-1-2. The AC signal is derived from two, phase locked, frequency synthesizers which allows phase shifting accuracy of 0.1 degree. Both are controlled on the IEEE-488 bus. The filling pulse is provided by an HP 116A pulse generator, which is also IEEE-488 controllable. The "bridge" used to balance the quiescent capacitance was fabricated "in-house" at General Electric by Dr. Andrew Ewvaraye.

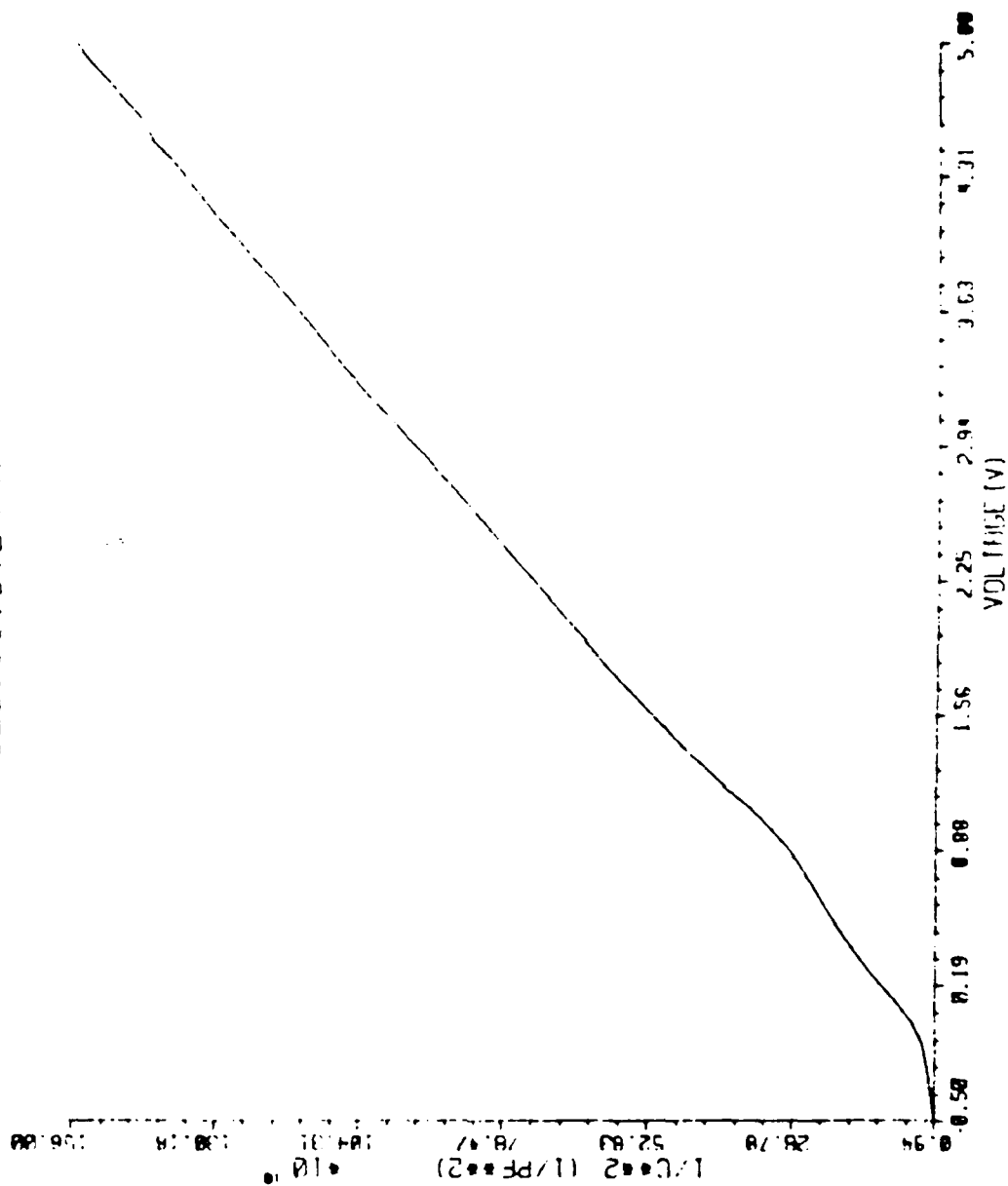
The signal is processed through an EG&G/PARC 115 preamplifier and combined with the phase shifted signal from the HP3336C at the mixer. (HP14541A) and the transient signal is then passed through an EG&G15 preamplifier to a Tracor-Northern TN-1710 signal averages. The TN-1710 captures the transient and outputs rate-window data to the LSI-11/23. Up to twenty-five rate windows may be programmed simultaneously on the TN-1710. The data is analyzed in a real-time, interactive program on a PRIME 850 computer.

Data may be acquired at any frequency between 10KHz and 20MHz. The data discussed in these results was taken at 20MHz.

3.1.3 Experimental Results

Three peaks were detected in the sample examined. These peak positions are associated with a $\tau_{\max} = 1.9 \text{ E-3}$. The activation

UES001.CVDATA



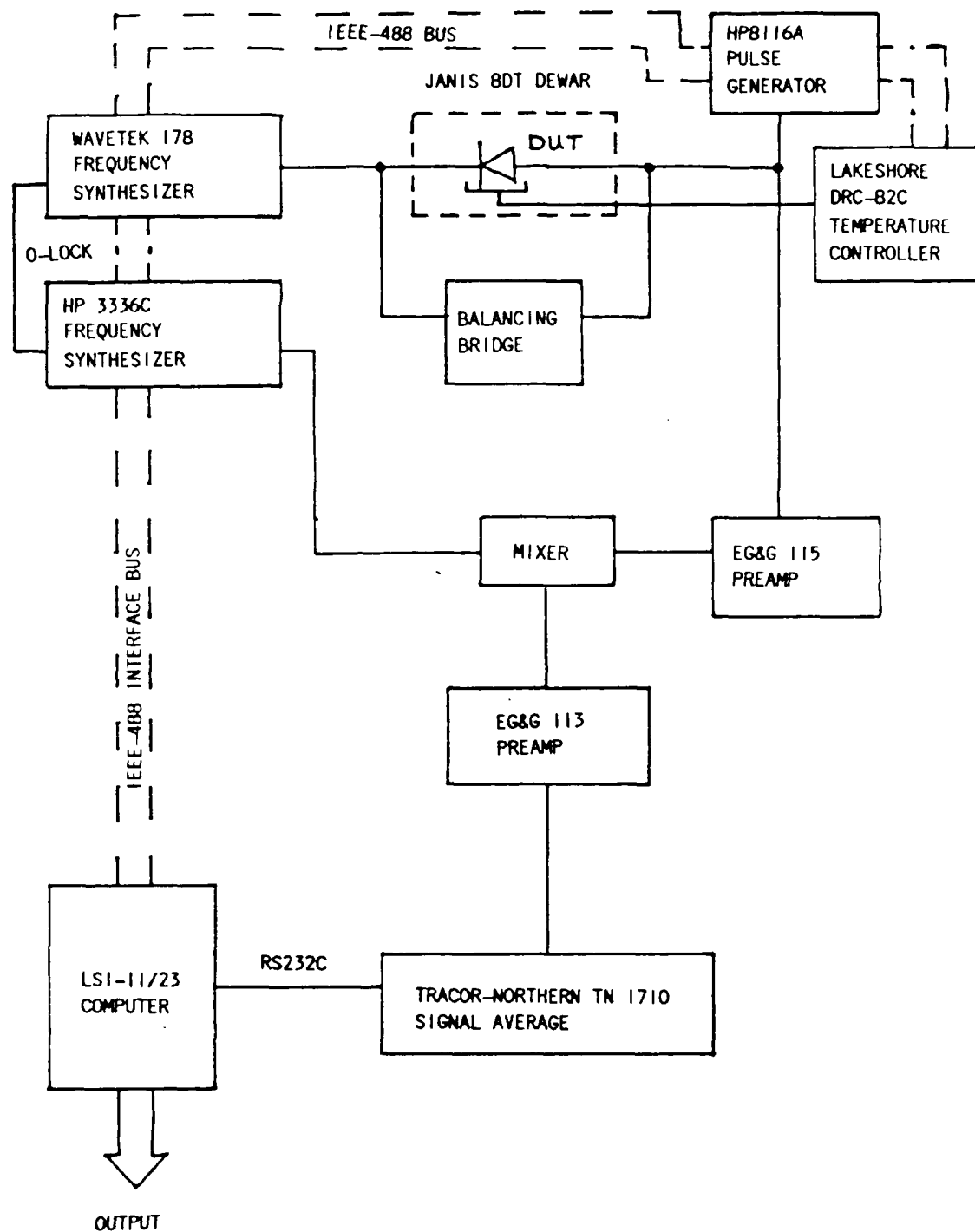


Figure 3-1-2 Equipment Block Diagram

energies calculated were 0.1 eV, 0.35 eV, and 0.54 eV respectively. The accepted literature value for the divacancy is $0.21 \pm .02$ eV.

The activation energies are calculated from an Arrhenius plot Figure 3-1-3 of $\ln(T^2 \tau_{\max})$ vs $1/KT$ by a linear regression fit. The spectrum is shown in Figure 3-1-4. The shoulder on the left of the V-O-C is probably due to the B-C complex, but could not be resolved well enough to calculate an energy. This peak is diminished due to the annealing of the sample after irradiation. The Arrhenius plot is shown in Figure 3-1-4.

3.2 DLTS UNIT NO. 2

Defects in 2MeV electron-irradiated silicon samples were analyzed using a Polaron DL4600 DLTS system over a temperature range of 90-300K. All DLTS scans were performed in darkness with decreasing temperature. The samples were analyzed prior to electron bombardment to determine the background residual impurities. No defect levels were found at concentrations exceeding 10^{12} cm^{-3} . The samples were then irradiated with 2MeV electrons near room temperature (300K) to $2 \times 10^{17} / \text{cm}^2$.

The thermal stability of the defects was determined by isochronal annealing, with 10-minute intervals, up to 450K in situ under a vacuum of 10^{-3} torr. Dry nitrogen atmosphere was used for higher temperatures, and the DLTS spectrum was measured after each stage of annealing.

We observed three distinct defects of comparable concentration that are produced by room-temperature electron irradiation in boron-doped FZ silicon. We tentatively correlated the high temperature trap at $E_V + 0.44$ eV with the carbon-interstitial + carbon-substitutional ($C_i + C_s$) pair identified by Brower,^[3-1] using EPR techniques, in electron-irradiated boron-doped silicon which contains carbon. Brower suggests that the pair is formed when a mobile carbon interstitial is trapped by a substitutional carbon atom. It can

ARRHENIUS PLOT FOR UES013

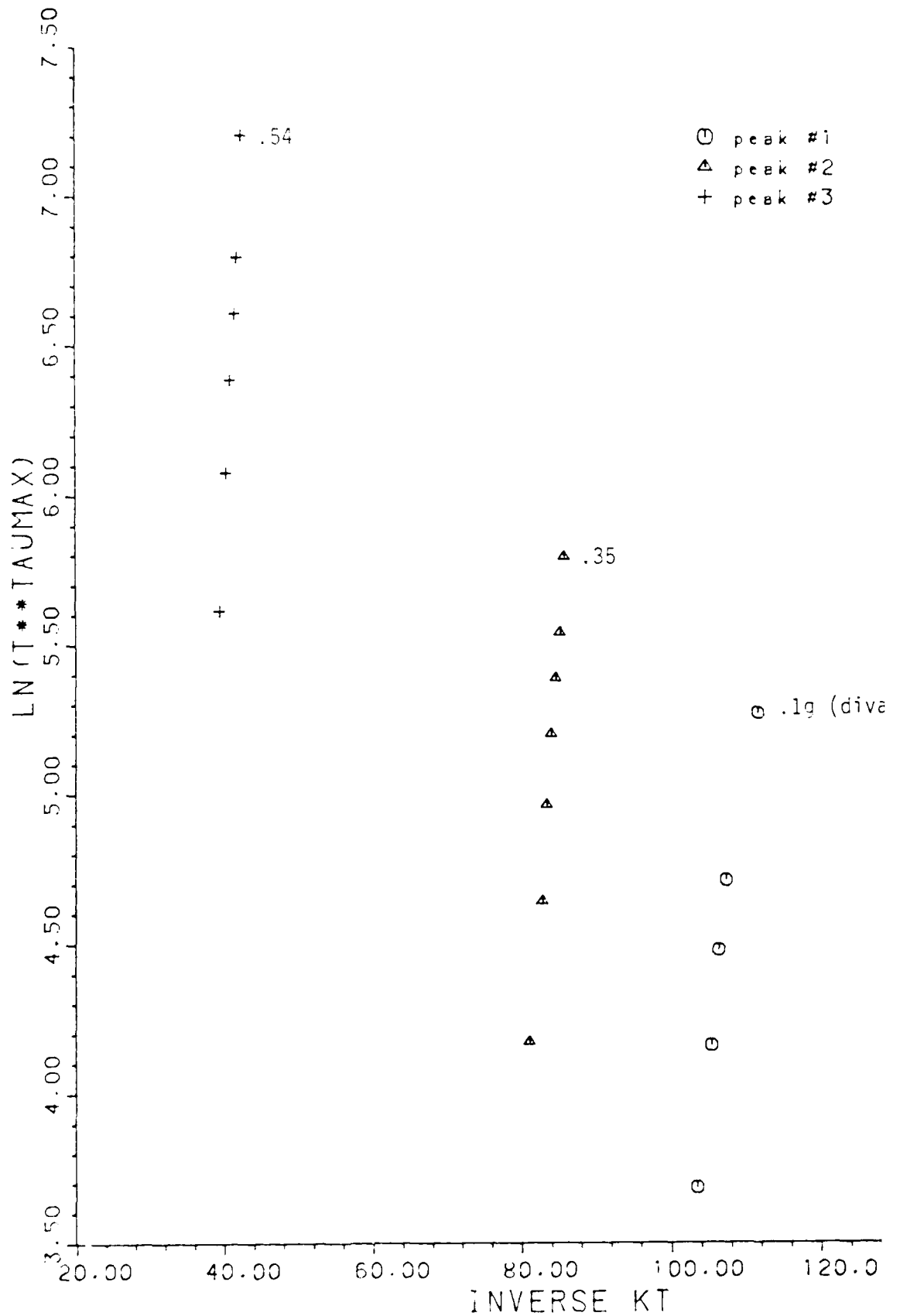
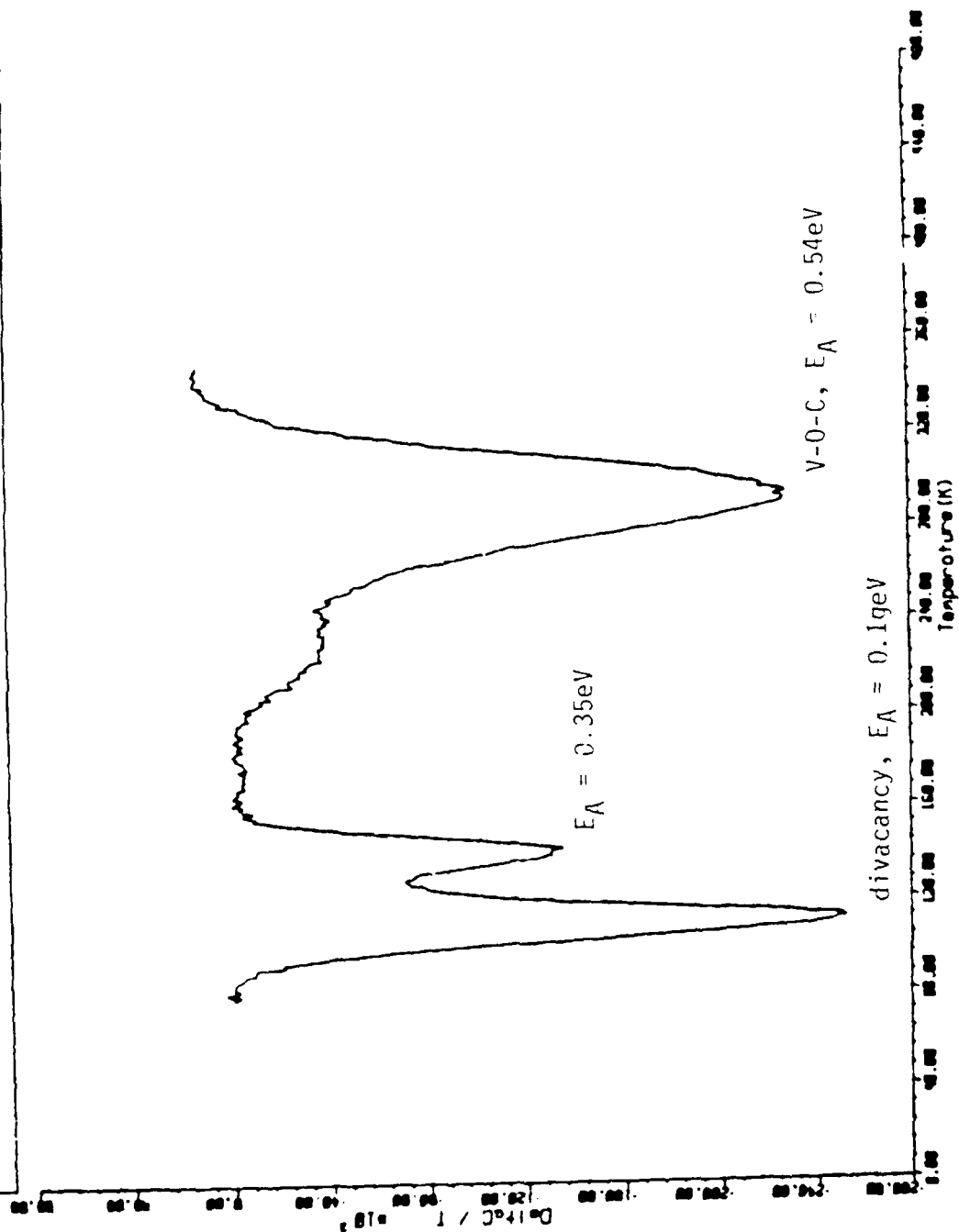


Figure 3-1-3 Arrhenius Plot 1

Sample ID: UES013 Date Run: 18-MAR-87
Window width: 0.01170 sec



be produced by either electron or neutron irradiation at room temperature. The pair was observed by Jaworowski et al.^[3-2] at $E_V + 0.39\text{eV}$ as the major DLTS peak after electron-irradiation of silicon with high concentration of substitutional carbon. Our correlation is based on the similar behavior under isochronal annealing showing the center disappearing at approximately 575K.

Figure 3-2-1 shows typical DLTS spectra for the two low temperature defects H_1 and H_2 measured with six different rate windows. Their thermal activation energies determined in the conventional manner (Figure 3-2-2) were $E_V + 0.15 \pm 0.02\text{ eV}$ and $E_V + 0.28 \pm 0.02\text{ eV}$ and they were detected in concentrations higher than $2 \times 10^{15}\text{ cm}^{-3}$. Capture cross-sections were not determined, and additional possible corrections for their temperature dependence are not included. Figure 3-2-3 shows results of isochronal annealing of H_1 and H_2 traps. Both traps anneal out rapidly between 500 and 550K.

The tentative identifications given here are based on comparison with energy levels and the thermal stability of defects previously observed in boron-doped silicon which had been electron-irradiated at near room temperature. The H_1 deep level corresponds to a positive state of the divacancy (V_2^+). Kimerling^[3-3] first correlated the H_1 peak with a positive charge of the divacancy which was firmly identified by Watkins and Corbett^[3-4] in their electron paramagnetic resonance experiment. The H_2 defect is most likely a boron related trap. If the impurity concentration is high, the mutual annihilation of the primary radiation defects, i.e., vacancies and interstitials decreases and the formation of complexes with the basic dopant increases. The activation energy of the H_2 is equal to that of the vacancy-oxygen-boron complex ($V-O-B$),^[3-5] which can be observed in F silicon after illumination at room temperature, but the ($V-O-B$) complex anneals out at 675K which is approximately 125K higher temperature than the annealing temperature of the H_2 defect. Chantre^[3-6] recently suggested the possibility of a room temperature stable boron-vacancy ($B-V$) pair. This is a new configurationally bistable center in quenched boron doped silicon. The observed thermal stability of the center (day

5000/s, 2000/s
 1000/s, 400/s
 200/s, 80/s



* 826-2.3 7711 3500 1010 87

* 154meV (2)

* 295meV (1)

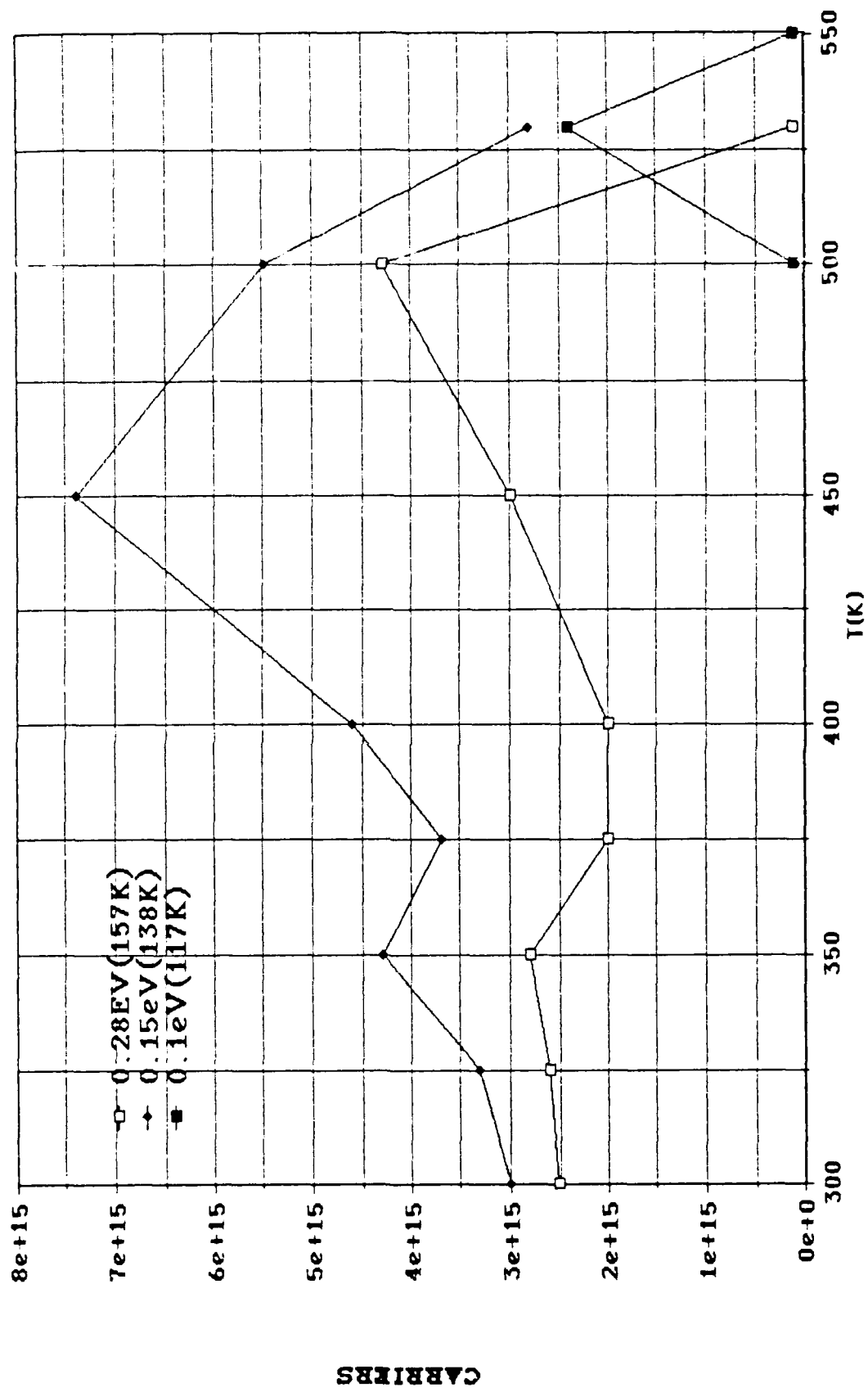


Figure 3-2-3 Peak Height vs. Temperature

at room temperature) seems to be in conflict with the observed annealing temperature for the H_2 (anneals out above 500K). The B-V pair may be unstable at room temperature in the presence of the high density of electrons and holes generated by 2MeV electron-irradiation. This would explain the nondetection of the bistable center^[3-6] in room temperature electron-irradiated boron-doped silicon. A prominent majority carrier trap was observed by Drevinsky and DeAngelis^[3-7] after electron-electron irradiation in FZ silicon heavily doped with boron (10^{17} cm^{-3}) at $E_v + 0.30\text{eV}$. They suggest a boron interstitial-boron substitutional pair (B_i-B_s) as a candidate structure.^[3-3] The annealing behavior of their center, however, is similar to the (V-O-B) center;^[3-5] their center does not anneal out until 675K.

The doping impurity level (B: $2 \times 10^{17} \text{ cm}^{-3}$) in our FZ silicon is much higher than the oxygen concentration (O: $2 \times 10^{15} \text{ cm}^{-3}$). This supports a possible assignment of H_2 to the boron interstitial-boron substitutional (B_i-B_s). A new deep level has appeared after the 500K annealing step and annealed out at 550K (Figure 3-2-3). Similar deep levels were observed in boron-doped silicon after the annealing of the divacancy at about 550K.^[3-5]

Recently, Londos and Banbury^[3-8,3-9] reported on DLTS and MCTS (minority-carrier-trap spectroscopy) studies for electron-irradiated boron-doped silicon. Song et al.^[3-10] observed using DLTS a configurational metastability of vacancy-related defects in electron-irradiated n-type silicon. These recent studies have raised a number of important new questions concerning the properties of primary radiation defects and their interactions in silicon.

3.3 HALL ANALYSIS

A 1cm by 1cm sample was taken from the electron irradiated silicon sample. The boron concentration was $1 \text{ E } 17 \text{ atoms/cm}^3$. Divacancies were introduced by electron bombardment (2MeV). We assumed a divacancy

creation factor of 0.01 divacancies for every electron. The intent was to produce as many divacancies as we had boron atoms.

Wires were indium soldered to the four corners of the 1cm by 1cm sample. This sample was intended to be used later for low temperature infrared absorption measurement; thus, no laser annealing was performed on the four contacts.

Hall data were taken from 23K to 380K. The low temperature results demonstrated some scatter in the data and poor r_1/r_2 values because we did not laser anneal the contacts. Because of this problem, we do not include data between 23K and 26K. If possible, at a later date, we shall redo this temperature range with laser annealed contacts.

The sample was p-type over the entire temperature range; indicating that the number of divacancies created did not equal the number of boron atoms present. The hole concentration as a function of $1000/T$ is presented in Figure 3-3-1.

The data were analyzed by fitting the charge balance equation. The high temperature data above 200K, which indicate the presence of a deeper level, were deleted for the initial fits. From these fits, we conclude the following concentrations for the elements of interest.

$$\begin{aligned}\text{Donor Concentration} &= 7.36 \text{ E } 15/\text{cm}^3 \\ \text{Boron Concentration} &= 2.40 \text{ E } 16/\text{cm}^3 \\ \text{2nd Acceptor Level Concentration} &= 9.61 \text{ E } 15/\text{cm}^3\end{aligned}$$

The activation energy of this second acceptor level is 0.034eV.

The calculated fit using these values is presented in Figure 3-3-2.

The next set of calculations used all the data to provide a fit. The parameters for donors and the first two acceptor levels did not change significantly. An activation energy of 0.182eV was indicated for

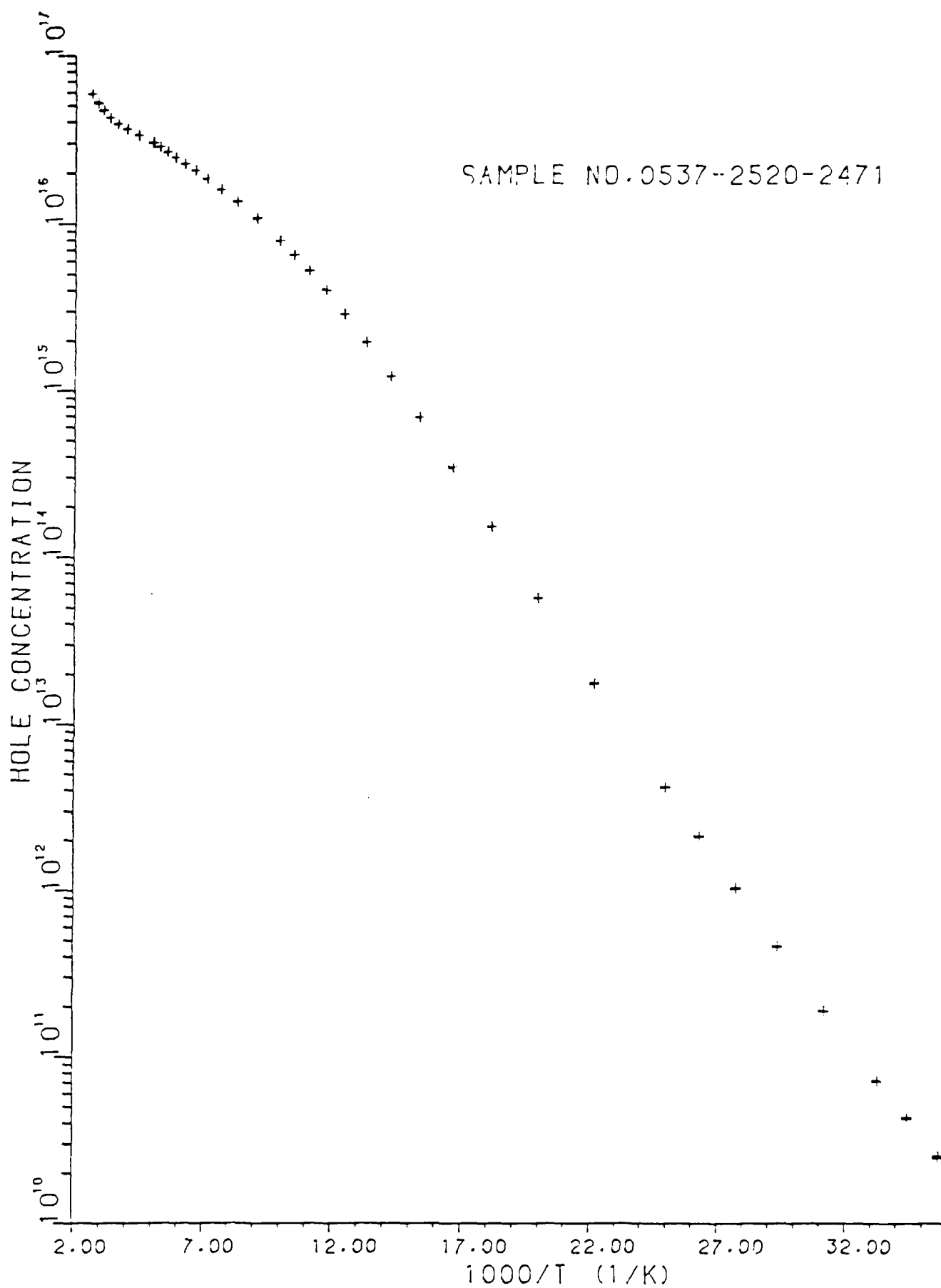


Figure 3-3-1 Hole Concentration vs. 1000/T

SAMPLE NO. 0537-2520-2471

THU, MAR 19 1987

SAMPLE TYPE: P-TYPE

MASS TYPE: LANG

R-FACTOR: NOT = 1

NLEVEL = 2

CHISQUARE = 0.82

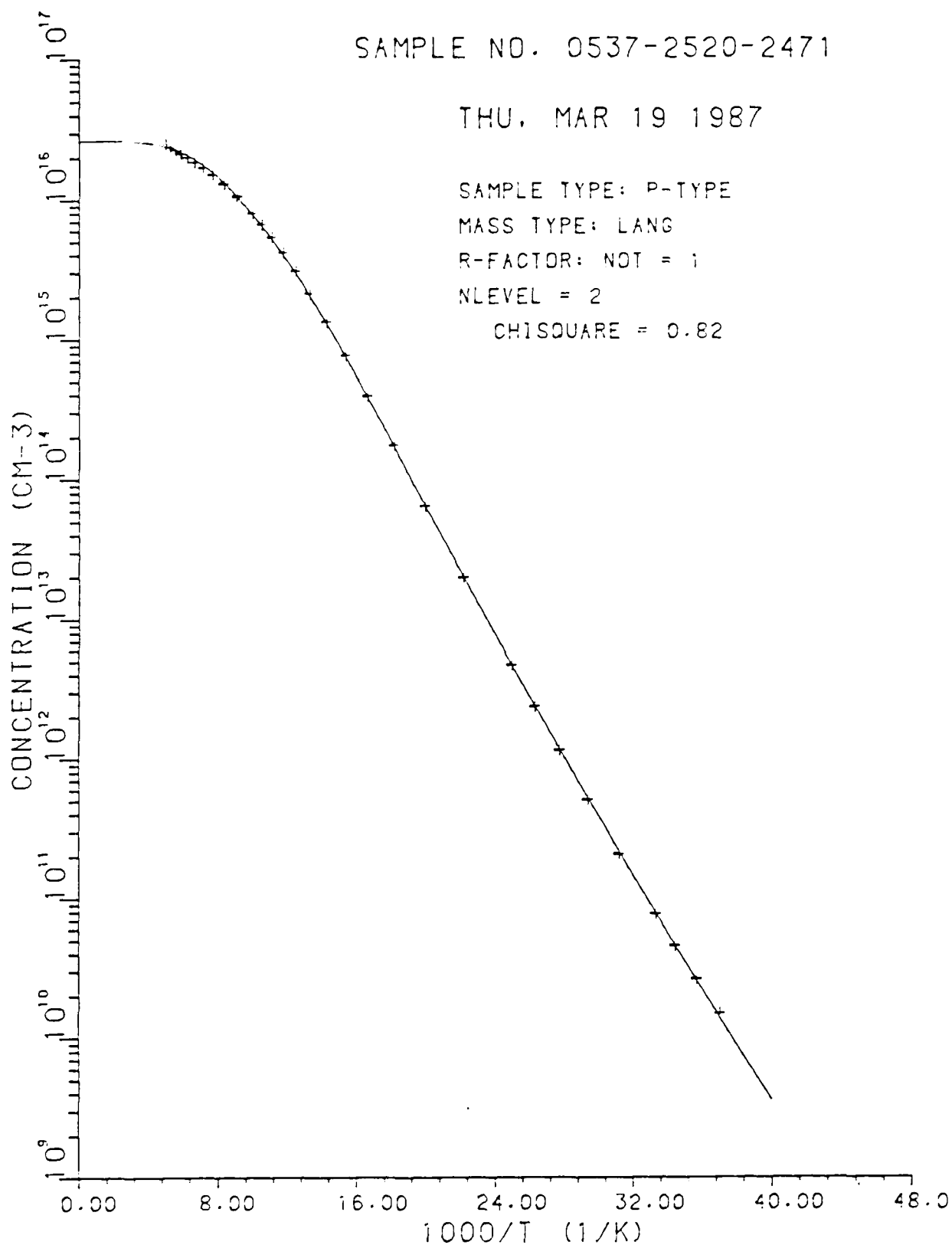


Figure 3-3-2 Calculated Fit

the deep level. This is within experimental error of the energy of 0.21eV generally associated with the divacancy.

We performed another set of calculations by fixing the energy of the divacancy at 0.21eV. In this case, the fit produced a χ^2 , which is a measure of how well the data have been fit, of 0.84. This compares with a χ^2 of 0.75 when all the parameters were allowed to vary. Both these fits may be considered to be equivalent.

The last fit which set the divacancy level at 0.21eV produced the trace shown in Figure 3-3-3. The parameters associated with this trace are listed below.

$$\begin{aligned}N_D &= 6.96 \text{ E } 15/\text{cm}^3 \\N_B &= 2.47 \text{ E } 16/\text{cm}^3 \\E_B &= 0.0469\text{eV} \\N_{A2} &= 8.98 \text{ E } 15/\text{cm}^3 \\E_{A2} &= 0.0339\text{eV} \\N_{A3} &= 3.14 \text{ E } 16/\text{cm}^3 \\E_{A3} &= 0.21\text{eV (Fixed)}\end{aligned}$$

3.4 INFRARED ANALYSIS

The infrared spectroscopic technique permits examination of the defects produced in silicon by 2MeV electron irradiation. Interstitial and vacancy defects extend the bandedge into the infrared when the sample is observed at 300K. These defects cause the normally sharp 1.06 micron bandedge to tail into the infrared to 1.4 microns. This tail can be annealed out only at 1200K heat treatment.

Observation at 300K also produces a band at 1.8 microns due to the neutral divacancy V_2^0 and/or the negative divacancy. When the Fermi level is below $E_c - 0.22\text{eV}$, the negative divacancy V_2^- contributes to the 1.8 micron band.

SAMPLE NO. 0537-2520-2471

FRI, MAR 20 1987

SAMPLE TYPE: P-TYPE

MASS TYPE: LANG

R-FACTOR: NOT = 1

NLEVEL = 3

CHISQUARE = 0.84

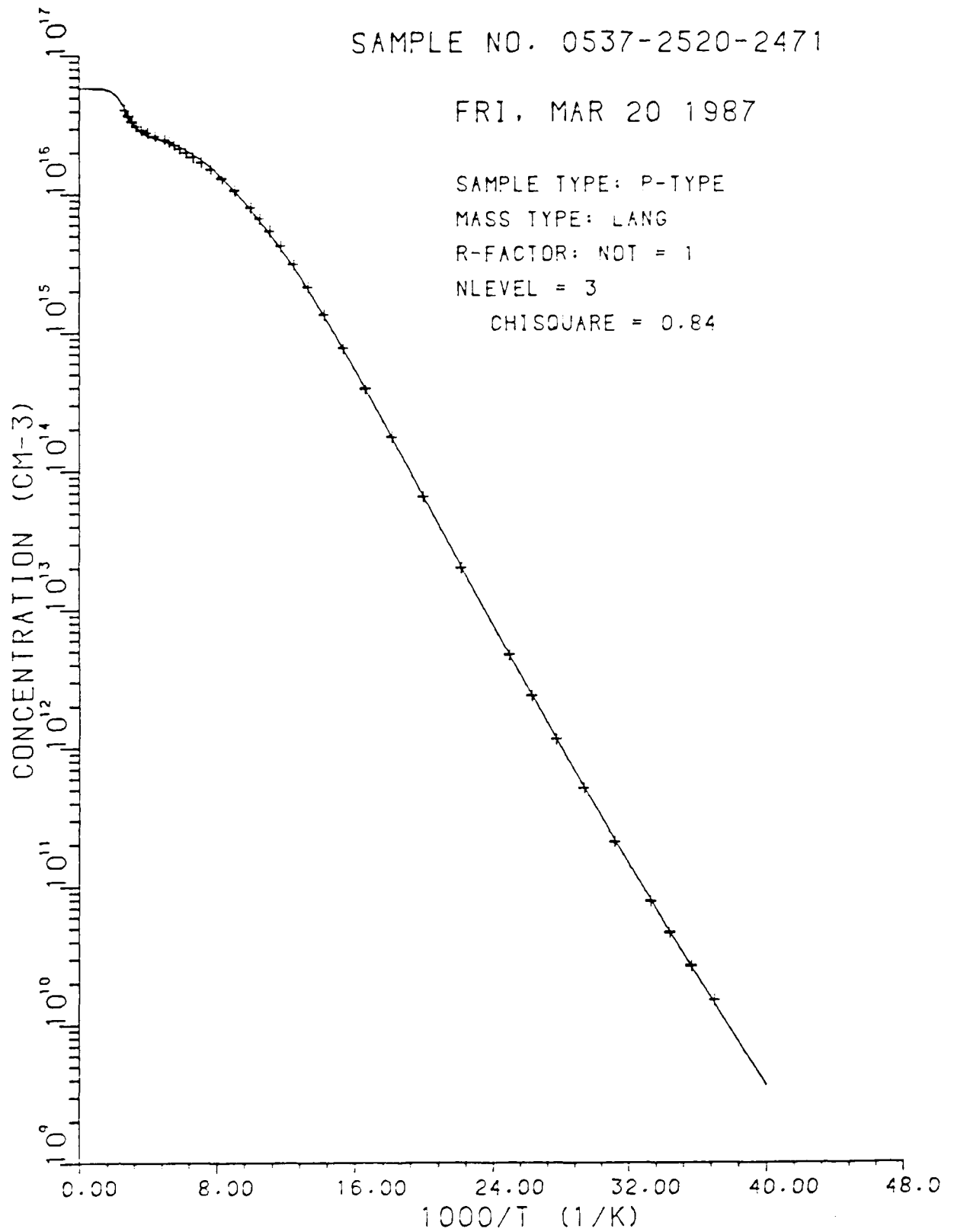
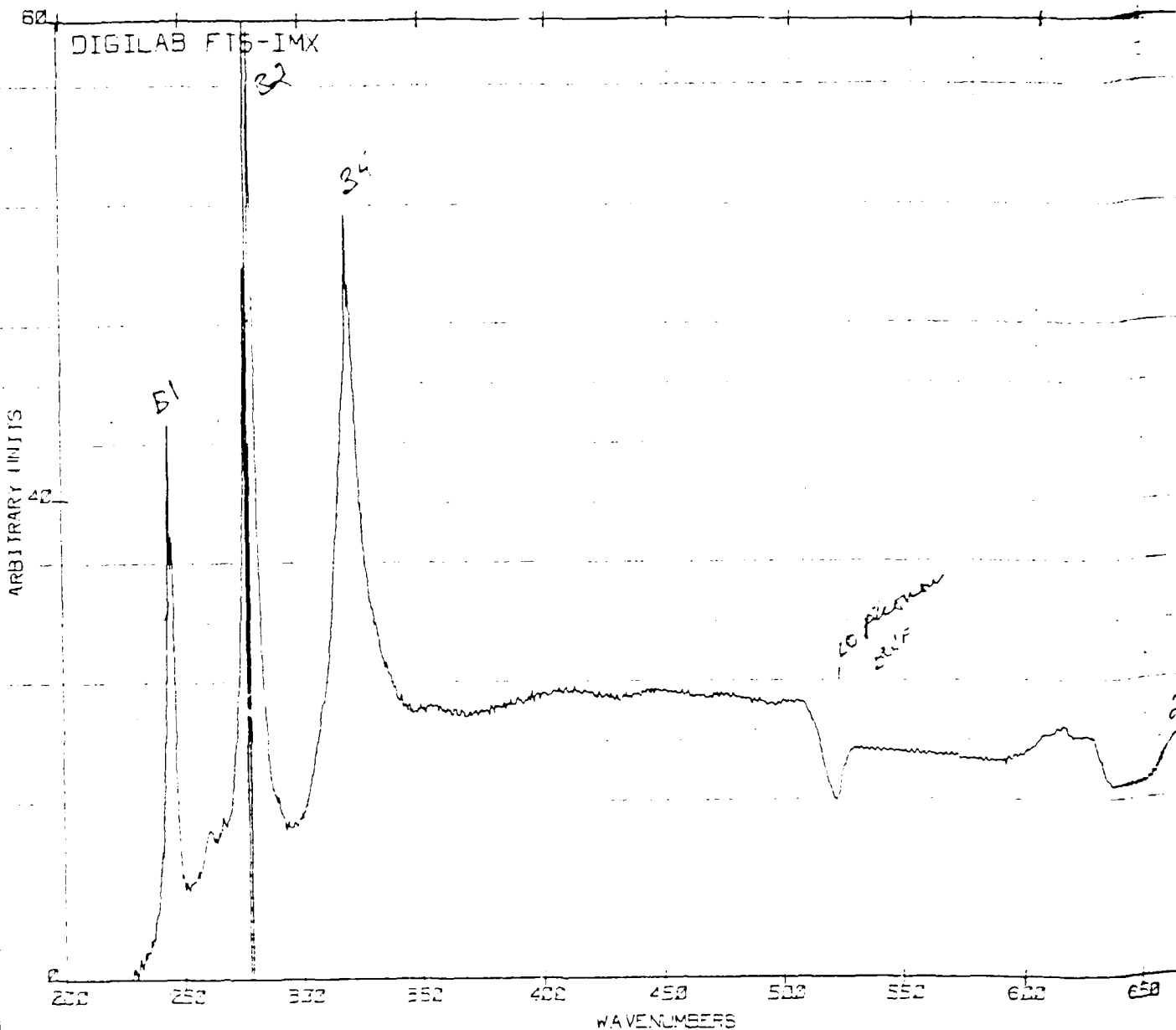


Figure 3-3-3 Calculated Fit $E_{A3} = 0.21\text{eV}$

When the Fermi level is above $E_c - 0.22\text{eV}$, the divacancy state shifts over to the double negative charged state $C_2^=$ and may be observed at 3.45 and 3.62 microns. Temperatures below 60K must be used to observe this state; the bands become sharper and more intense as the temperature is decreased below 60K. The position of the Fermi level will determine the relative strength of the 1.8 micron and the 3.45, 3.62 micron bands. As stated, the Fermi level must be above $E_c - 0.22\text{eV}$ to populate the double negative charged state. Thus, to observe the strongest photoconductivity signal at the 4 micron band position, this condition must be met.

The infrared analysis presented for our electron irradiated samples can not provide an exact value for the boron concentration because the concentration is too high ($1 \text{ E } 17 \text{ atoms/cm}^3$). The far infrared curve of Figure 3-4-1 shows the reversal of the spectral lines indicating the high boron content. Phosphorus content can normally be observed by illuminating the sample in the course the scan. No phosphorus was observed; this indicates that the multipass zoning did successfully remove phosphorus. There can be no lower level for the phosphorus content because the boron content was so high. Normally we desire low levels for boron to obtain a good limit of detection statement of phosphorus.

The main curve of interest is produced in Figure 3-4-2. This presents evidence of the V_2^+ center for the divacancy at 2500 cm^{-1} . This spectra also was produced at a temperature of 5K. The concentration of divacancies was not greater than the boron concentration; however we were successful in observing the defect structure desired. The divacancies which were produced were compensated by the boron in the crystal and thus exposed the V_2^+ state. The boron concentration was $1 \text{ E } 17 \text{ cm}^{-3}$ which was about 25 times the divacancy concentration. The DLTS analysis gave a boron value of $3.8 \text{ E } 16/\text{cm}^{-3}$ for boron and the Hall data gave a value of $2.4 \text{ E } 16/\text{cm}^{-3}$. This compares with an infrared value of $1 \text{ E } 15/\text{cm}^{-3}$ for the V_2^+ state.



SFL=61B2471AAD
NSCAN=500
PLMPS

3/24/87 113

Figure 3-4-1 Boron Spectra (5K)

LAB FILAB FIS-IMK

APR 01 1967
FIS-IMK
FILAB

0.00000

WAVELENGTHS

2200 2250 2300 2350 2400 2450 2500 2550 2600 2650 2700 2750 2800 2850 2900 2950 3000 3050 3100 3150 3200 3250 3300 3350 3400 3450 3500 3550 3600 3650 3700 3750 3800 3850 3900 3950 4000 4050 4100 4150 4200 4250 4300 4350 4400 4450 4500 4550 4600 4650 4700 4750 4800 4850 4900 4950 5000 5050 5100 5150 5200 5250 5300 5350 5400 5450 5500 5550 5600 5650 5700 5750 5800 5850 5900 5950 6000 6050 6100 6150 6200 6250 6300 6350 6400 6450 6500 6550 6600 6650 6700 6750 6800 6850 6900 6950 7000 7050 7100 7150 7200 7250 7300 7350 7400 7450 7500 7550 7600 7650 7700 7750 7800 7850 7900 7950 8000 8050 8100 8150 8200 8250 8300 8350 8400 8450 8500 8550 8600 8650 8700 8750 8800 8850 8900 8950 9000 9050 9100 9150 9200 9250 9300 9350 9400 9450 9500 9550 9600 9650 9700 9750 9800 9850 9900 9950 10000

SFL-5152471BAC
NISCANS-500
FILM-5

3'24'07 12:22:25

The V_2^+ state observed is the desired level; it results from the compensation of the boron atoms. We do not observe neutral or negatively charged divacancies because boron has performed its desired role of compensation. The intensity of the positive divacancy would be greater if we had a great dose of electrons. The desired level would be an equal concentration of divacancies and boron atoms. The interesting fine tuning experiments in which the concentrations are varies about this exact compensation value are beyond the scope of this Phase I effort.

An attempt was made to illuminate the sample at the same time the spectra was taken. There was no change in the intensity of the positive divacancy and no neutral divacancies or negative divacancies were created. This provides important evidence that the counterdoping theory of Elliott^[1-1] is correct; infrared detectors may be created by counterdoping and are stable under illumination.

4.0 APPLICATION OF MULTIVALENT STATISTICS TO COUNTERDOPED DETECTORS

4.1 INTRODUCTION

Most impurities that are contemplated for their use as either deep donor or acceptor in the counterdoped infrared detector supply several other energy levels in the gap. The multivalent nature of these centers has never been incorporated in a study of the expected detector response. In particular, these levels may be ordered in the usual donor-acceptor ascending order of energy levels; or they may be reverse ordered as is characteristic of the negative -U center. The consequences of the level ordering and the multivalent nature of these impurities is the subject of the following theoretical analysis.

4.2 THE DIVACANCY

The divacancy in silicon introduces several levels in the energy gap of the host lattice. In p-type silicon the first level nearest the valence band is the donor level associated with the charge transition.

$${}^+V_2 \longrightarrow V_2^0, \quad (4-1)$$

which may occur with the emission of a hole to the valence band, or by capture of an electron from the conduction band. The second level of interest is the level corresponding to the transition.

$$V_2^0 \longrightarrow V_2^-. \quad (4-2)$$

The divacancy can also carry one more negative charge in the transition.

$$V_2^- \longrightarrow V_2^{--}. \quad (4-3)$$

All these charge states are realizable in equilibrium as the Fermi level is raised, or in a non-equilibrium experiment via carrier injection. Figure 4-1 illustrates the present state of knowledge about the divacancy levels in silicon.^[4-1]

The transition in Equation 4-1 is important for the operation of the counterdoped detector. It is of interest to study the effect of the next charge state, V_2^- in Equation 4-2, on the detector performance. The model used so far has included only the lowest donor level of the divacancy.^[4-2] Here, the next divacancy level will be considered and incorporated into the model. For the sake of generality, the initial developments will apply to any counterdoped system with two charge states in the gap. Reference 4-2 is included as Appendix 1 for your information. The theory developed in this reference has a bearing on the total picture of counterdoped detectors. Extended experimental research is necessary to test the predictions presented in this theory.

4.3 MULTIVALENT STATISTICS

We must start first with the statistics of multivalent levels. This subject has been covered extensively by Shockley and Last,^[4-3] Blakemore,^[4-4] and Look.^[4-5] Let the state of the impurity with no ionizable electrons be the zeroth state of the impurity. This state will have the total energy which will be set to zero, $\epsilon_0 = 0$, and the degeneracy γ_0 . The state with k ionizable electrons will be denoted with the subscript k ; ϵ_k and γ_k , for the total energies and degeneracies, respectively. In the case of the divacancy in silicon, the $k = 0$ state is the positively charged divacancy V_2^+ , the $k = 1$ state is the neutral divacancy V_2^0 , etc. The energy needed to change the charge state $+1/0$ is $\epsilon_1 - \epsilon_0$. This energy will promote an electron from the valence band to the first level in the gap (the 0.204eV level in Figure 4-1).

It is understood that the system cannot support any other charge states in the gap. For example, the triply negative charge state $V_2^{=}$ would be a resonance in the conduction band and as such an autoionizing system. The extra electron would be at the bottom of the conduction band rather than on the divacancy. Similarly, the double positively charged state V_2^{++} is a resonance in the valence band, or below, so that it takes more than the bandgap energy to remove an electron from the V_2^+ charge state. That is why V_2^+ has no

ionizable electrons and why it takes no energy to transfer one electron from the valence band to form V_2^+ . By the same token, simple donors in silicon have either four or five outer shell electrons in the D^+ and D^0 charge states respectively. Only one electron is ionizable though in the D^0 configuration.

The occupancy of N impurities with k ionizable electrons can be derived most simply by the maximum probability method. The number of impurities with k ionizable electrons is given by Equation B26 of reference.^[4-5]

$$n_k = \frac{N}{1 + \sum (\gamma_l / \gamma_k) \exp [\epsilon_k - \epsilon_l - (k-l)\mu] / kT} \quad (4-4)$$

where μ = chemical potential
 k = Boltzman constant
 T = absolute temperature

As emphasized by Look^[4-5], the relevant parameters are the relative degeneracy factors, γ_l / γ_k , and the differences in total energies, $\epsilon_l - \epsilon_k$. The relevant parameters are not the single electron energy levels.

Equivalently, the ratio of concentrations

$$\frac{n_k}{n_{k-1}} = \frac{\gamma_k}{\gamma_{k-1}} \exp \frac{(\mu - \epsilon_k)}{kT} \quad (4-4a)$$

where ϵ_k is the energy required to take the k th electron from the valence band and place it onto the defect with $k-1$ electrons already present, i.e.,

$$E_k = \epsilon_k - \epsilon_{k-1} \equiv E(k/k-1) \quad (4-4b)$$

The new symbol $E(k/k-1)$ gives the "before" and "after" picture of the number of ionizable electrons on the defect. We shall also use the symbol

$$g_k = \gamma_k / \gamma_{k-1} \quad (4-4c)$$

for the "relative" degeneracy of a level.

Exploration of the detector response of a multivalent impurity system offers an intriguing possibility of contemplating the behavior of a negative $-U$ system.^[4-6 to 4-11] In these systems, the total energy of the $k+1$ electron configuration is lower than the configuration with k electrons.

$$\epsilon_{k+1} < \epsilon_k \quad (4-5)$$

It is as if the extra electron was attracted rather than repelled from the k electrons already on the impurity. In fact, it is the Jahn-Teller relaxation of the defect in the $(k+1)$ charge state which lowers the electronic energy while raising the elastic energy. The overall gain in energy is negative, hence the negative $-U$ property of the center.

4.4 CHARGE BALANCE FOR THE DIVACANCY

In the case of the divacancy system, the charge balance equation will be

$$n + N^- + 2N^= + N_A^- = p + N_D^+ + N^+ \quad , \quad (4-6)$$

where

- n = density of electron in the conduction band
- $N^+ = n_0$ = density of positively charged divacancies
- $N^0 = n_1$ = density of neutral divacancies
- $N^- = n_2$ = density of negatively charged divacancies
- $N^= = n_3$ = density of doubly negative charged divacancies
- p = density of holes in the valence band
- N_A = density of the counterdopant, here boron
- N_D = density of the shallow donors

The conservation of divacancies accounts for the total density of divacancies

$$N = N^+ + N^0 + N^- + N^- \quad (4-7)$$

4.5 DEGENERACY

Next, we must determine the degeneracy of the divacancy charge states and their total energy for input into Equations 4-4, 4-6, and 4-7. The easiest task is to determine the relevant total energies since these are experimentally measured. In the notation of Equation 4-4 and Figure 4-1,

$$\epsilon_0 = 0 \quad (4-8)$$

$$\epsilon_1 = E_1 = 0.204\text{eV} = E_D$$

$$\epsilon_2 = E_1 + E_2 = 0.93\text{eV} = E_D + E_{DA}$$

$$\epsilon_3 = E_1 + E_2 + E_3 = 1.8\text{eV} = E_D + E_{DA} + E_{DAA}$$

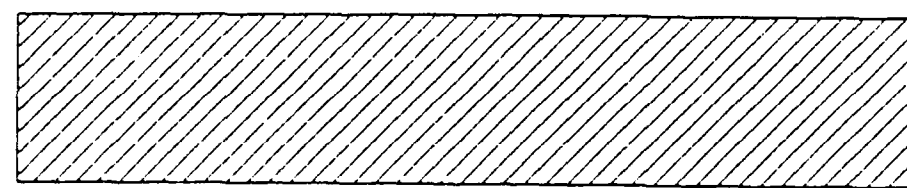
where E_k is the energy necessary to add the k th electron from the valence band to the $(k-1)$ charge state of the divacancy.

Explicitly we have using Equation 4-4,

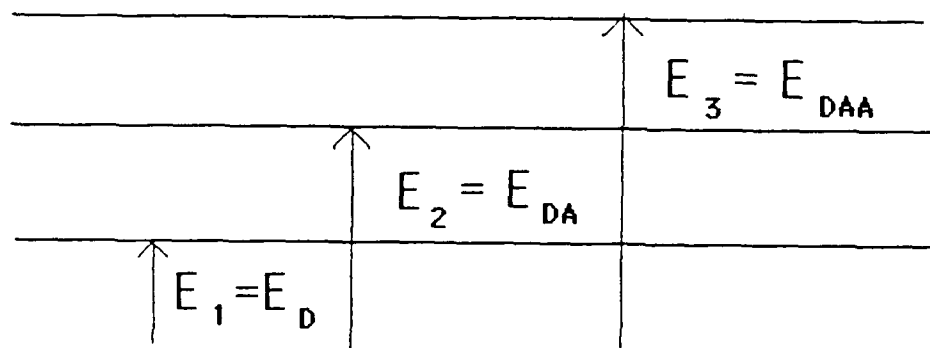
$$n_0 = \frac{N}{1 + \frac{\gamma_1}{\gamma_0} \exp\left[\frac{(\mu - E_1)}{kT}\right] + \frac{\gamma_2}{\gamma_0} \exp\left[\frac{(2\mu - E_1 - E_2)}{kT}\right]} = N^+ \quad (4-9a)$$

$$n_1 = \frac{N}{1 + \frac{\gamma_0}{\gamma_1} \exp\left[\frac{(E_1 - \mu)}{kT}\right] + \frac{\gamma_2}{\gamma_1} \exp\left[\frac{(\mu - E_2)}{kT}\right]} = N^0 \quad (4-9b)$$

$$n_2 = \frac{N}{1 + \frac{\gamma_0}{\gamma_2} \exp\left[\frac{(E_1 + E_2 - 2\mu)}{kT}\right] + \frac{\gamma_1}{\gamma_2} \exp\left[\frac{(E_2 - \mu)}{kT}\right]} = N^- \quad (4-9c)$$



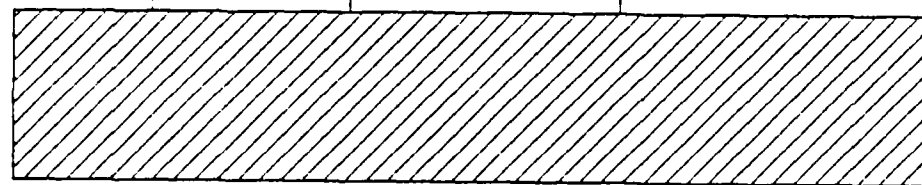
CB



(--/-) 0.9

(-/0) 0.75

(0/+) 0.2



VB

Figure 4-1 Levels of Divacancy in Silicon

where the $N^- = n_3$ state has been dropped out for physical reasons (low occupancy level at the temperatures of interest).

The degeneracy factors in Equations 4-4c and 4-9,a,b,c depend on the detailed electronic structure of the divacancy. Imagine two nearest neighbor silicon atoms in the diamond structure. Each of the atoms have three other silicon nearest neighbor atoms. Bonds connecting every pair of atoms have two electrons since each atom contributes four electrons for bonding. When two atoms are removed, a divacancy is created. The bonds with six remaining atoms are broken, and there are six dangling bonds pointing toward the position of the divacancy. In the Watkins-Corbett model,^[4-12] we find two pairs of atoms rebonding; this ties up four electrons and leaves two loosely bound electrons representing the neutral state of the divacancy, V_2^0 . The bonding state of these loosely bound electrons accommodates either one electron in the V_2^+ charge state, or, as mentioned above, two electrons in the V_2^0 state. Two additional electrons can be placed in the antibonding combination of the two dangling orbitals to produce in succession the V_2^- and $V_2^{=}$ charge states.

The symmetry point group of the undistorted divacancy would be D_{3d} . The Jahn-Teller distortion lifts the electronic degeneracy, resulting in a rebonding of the two atom pairs; thus, the symmetry is reduced to that of the C_{2h} point group. The degeneracy of each level is two-fold counting the spin. The energy level diagram for the four charge states is given in Figure 4-2.

In Figure 4-2, the number of ways the given number of electrons can be placed gives the degeneracy factor. In order to avoid confusion, note that the lone electron in the V_2^+ state is not an ionizable electron. It takes more energy to ionize it than to promote a valence electron to the conduction band.

The V_2^+ and V_2^- states have unpaired electrons and are Electron Paramagnetic Resonance (EPR) active. They were observed by Watkins and Corbett.^[4-12] There are newer models of the

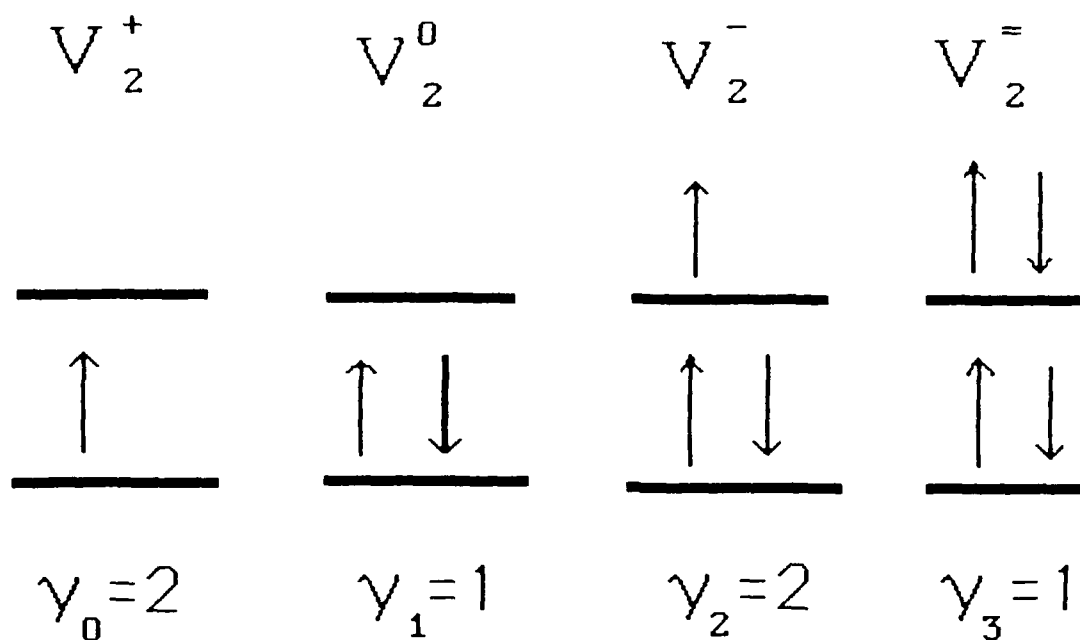


Figure 4-2 Electron Occupancy of the Dangling Bond States of the Divacancy and the Divacancy and the Associated Degeneracy Factors

divacancy;^[4-13] however, much work remains to elucidate all of its properties. The Watkins-Corbett model is sufficient for the accuracy of the present calculations.

We shall define the degeneracy factor g as

$$g_D = \frac{\gamma_1}{\gamma_0} = 1/2, \quad (4-10a)$$

$$g_{DA} = \frac{\gamma_2}{\gamma_0} = 1, \quad (4-10b)$$

$$g_{DAA} = \frac{\gamma_3}{\gamma_0} = 1/2, \quad (4-10c)$$

For simple acceptors $\gamma_0 = 4, \gamma_1 = 1$ thus $g = 1/4$

For simple donors $\gamma_0 = 1, \gamma_1 = 2$ thus $g = 2$

4.6 RATE EQUATIONS

It will be assumed that the first three charge states of the impurity will be sufficiently occupied at the temperature of interest (near liquid nitrogen temperature). This also implies that the two electronic levels involved, $0/+$ and $-/0$, can communicate only with the valence band. The rate at which the density of the charged defects changes is given by

$$\frac{\partial N^+}{\partial t} = B(0/+)N^0 p - A(0/+)N^+ \quad (4-11)$$

The first term is due to hole capture by N^0 and the second term is the result of hole emission to the valence band. The B coefficient is the recombination coefficient for the indicated charge state transformation. The A coefficient is the generation coefficient for neutral impurities.

$$\frac{\partial N^0}{\partial t} = A(0/+)N^+ - B(0/+)N^0 p - A(-/0)N^0 + B(-/0)N^- p. \quad (4-12)$$

The first two terms are as defined in Equation 4-11. The third term is the result of hole emission, while the fourth term is due to hole capture for the negatively charged species.

$$\frac{\partial N^-}{\partial t} = A(-/0)N^0 - B(-/0)N^- p + (\text{neglected terms}) . \quad (4-13)$$

The neglected terms involve (=/-) conversion.

These equations are supplemented by the charge neutrality condition,

$$p + N^+ = N_{\bar{B}} + N^- , \quad (4-14)$$

where $N_{\bar{B}}$ is the density of a shallow counter dopant, in this case boron. The "conservation" of divacancies completes the picture.

$$N = N^+ + N^0 + N^- . \quad (4-15)$$

The time derivatives in Equations 4-11 to 4-13 are zero for the steady state condition; thus, we may use Equations 4-11 to 4-13 to obtain.

$$A_D \equiv A(0/+)=B(0/+) \frac{N^0}{N^+} p , \quad (4-16)$$

$$A_{DA} \equiv A(-/0)=B(-/0) \frac{N^-}{N^0} p . \quad (4-17)$$

In thermal equilibrium, we have

$$p = N_V \exp (-\mu/kT) \quad (4-18)$$

where N_V is the effective density of states. Using Equation 4-4a, we see that

$$N^0/N^+ = n_1/n_0 = (\gamma^0/\gamma^+) \exp \left[\frac{(\mu - E_{DA})}{kT} \right] , \quad (4-19)$$

$$N^-/N^0 = n_2/n_1 = (\gamma^-/\gamma^0) \exp \frac{\mu - E_{DA}}{kT} . \quad (4-20)$$

Thus the relationship between the thermal generation coefficients A and the recombination coefficient B become.

$$A_D = N_V B_D g_D \exp\left(\frac{-E_D}{kT}\right) \quad (4-21)$$

$$A_{DA} = N_V B_{DA} g_{DA} \exp\left(\frac{E_{DA}}{kT}\right) \quad (4-22)$$

Using Equations 4-21 and 4-22 we may now rewrite Equations 4-11 to 4-13 and add the optical generation terms. Equation 4-11 picks up

$$- \langle \sigma_D \phi \rangle N_D^+ \quad (4-23)$$

Equation 4-12 picks up

$$\langle \sigma_D \phi \rangle N_D^+ - \langle \sigma_{DA} \phi \rangle N_D^0 \quad (4-24)$$

Equation 4-13 picks up

$$\langle \sigma_{DA} \phi \rangle N_D^0 \quad (4-25)$$

The σ 's are photon absorption cross-sections and ϕ is the photon flux. The brackets are spectral integrals.

It is convenient to define

$$\alpha_D = g_D N_V \exp(-E_D/kT) + \langle \sigma_D \phi \rangle / B_D \quad (4-26)$$

$$\alpha_{DA} = g_{DA} N_V \exp(-E_{DA}/kT) + \langle \sigma_{DA} \phi \rangle / B_{DA} \quad (4-27)$$

In terms of quantities just defined the steady-state concentrations of the charge states of the divacancy are

$$N^+ = \frac{N p^2}{p^2 + \alpha_D p + \alpha_{DA}} \quad (4-28)$$

$$N^0 = \frac{\alpha_D p N}{p^2 + \alpha_D p + \alpha_{DA}} \quad (4-29)$$

$$N^- = \frac{\alpha_D \alpha_{DA} N}{p^2 + \alpha_D p + \alpha_{DA}} \quad (4-30)$$

In fact, these equations are simply related to Equations 4-9a to 4-9c. The solution of Equations 4-28 to 4-30 depends on the density of holes p at the given temperature. That comes from the charge balance Equation 4-14 supplemented by the equation for the density of ionized acceptors (Equation 4-4a),

$$N_A^-/N_A^0 = (\gamma_A^-/\gamma_A^0) \exp\left[\frac{(\mu - E_A)}{kT}\right] \quad (4-31)$$

The acceptor level is two-fold degenerate with three electrons in it, when it is neutral. It is nondegenerate when it has four electrons and is negatively charged ($\gamma_A^- = 1, \gamma_A^0 = 4$). Thus

$$N_A^- = \frac{N_A}{1 + 4 \exp[(E_A - \mu)/kT]} \quad (4-32)$$

A rate equation for the counterdopant gives rise to

$$N_A^- = \frac{\alpha_A N_A}{p + \alpha_A} \quad (4-33)$$

where
$$\alpha_A = \frac{(N_V)}{4} \exp - (E_A/kT) + \langle \sigma_A \phi \rangle / B_A$$

Using the charge balance equation (Equation 4-17), we obtain a quartic equation for p

$$p^4 + p^3 (\alpha_A + \alpha_D + N) + p^2 [\alpha_D (\alpha_A + \alpha_{DA}) + \alpha_A (N - N_A)] + p \alpha_D (\alpha_{DA} \alpha_A - N \alpha_{DA} - N_A \alpha_A) - \alpha_{DA} \alpha_D \alpha_A (N_A + N) = 0 \quad (4-34)$$

If we set $\alpha_{DA} = 0$, we obtain the equation for the case of a singly ionizable deep donor. [4-2]

4.7 DETECTOR RESPONSE

Equation 4-34 can be solved at any temperature for any desired flux level corresponding to the given operating condition of the detector,

$$p = p(\phi, T) \quad (4-35)$$

The detector responsivity is given by 4-2, and 4-15

$$R \sim \left(\frac{\partial p}{\partial \phi} \right) \phi = \gamma \phi \quad (4-36)$$

where ϕ_B is the background level flux .

The detector's detectivity is then proportional to

$$D^* \sim \left(\frac{R}{p} \right)^{1/2} \quad (4-37)$$

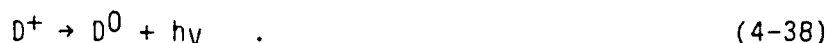
The results which will be displayed below have been obtained using the numerical input summarized in Table 4-1.

TABLE 4-1. INPUT PARAMETERS FOR THE CALCULATION OF THE DETECTOR RESPONSE
(FLUX $\phi_B = 0$ or $\phi_B = 10^{16}$ PROTONS/cm²-sec)

	Donor Level of the Deep Donor	Acceptor Level of the Deep Donor	Shallow Acceptor
Energy(eV)	$E_D=0.200$	$E_{DA}=0.75$ and allowed to vary	$E_A=0.044$
Degeneracy	$g_D = \left(\frac{\gamma^0}{\gamma^+} \right) = 1/2$	$g_{DA} = \left(\frac{\gamma^-}{\gamma^0} \right) = 2$	$g_A = \left(\frac{\gamma_A^0}{\gamma_A^-} \right) = 4$
Photon Absorption Cross Section (cm ²)	$\sigma_D = 5.4 \times 10^{-16}$	$\sigma_{DA} = 5.4 \times 10^{-16}$	$\sigma_A = 1.8 \times 10^{-15}$
Recombination Coefficient (cm ³ /sec)	$B_D = (6 \times 10^{-6} / T^{1.5})$	$B_{DA} = (6 \times 10^{-4} / T^{1.5})$	$B_A = (6 \times 10^{-4} / T^{1.5})$
Concentration (cm ³)	$N_D = 5 \times 10^{16}$		$N_A = 5 \times 10^{12}$ or $N_A = 5 \times 10^{16}$

The system will be investigated for a variety of situations. First, the system will be explored in thermal equilibrium. This means the light will be off, and we shall study both high and low counterdopant concentrations. In order to explore the consequences of the negative $-U$ properties, the E_{DA} energy will be allowed to vary from $E_{DA} > E_D$ to $E_{DA} < E_D$. The same properties will then be investigated in the presence of the background flux.

Figure 4-3 provides charge center concentrations in the absence of illumination and very low counterdopant boron concentration ($\phi_B = 0$, $N_B = 5 \times 10^{12}$). The positive $-U$ is the result. $E_{DA} = 0.3 \text{ eV}$ and $E_D = 0.225 \text{ eV}$ show that the deep donor, $E_D = 0.2 \text{ eV}$, exists primarily in its neutral charge state. Boron is totally compensated in the 200K temperature range. Initially, $N_D^+ = N_B$, but as the temperature rises electrons are promoted thermally to the $(-/0)$ acceptor level and a hole is created in the valence band. This transition is more likely than the transformation $(0/+)$



This is true because there are many more N_D^0 than N_D^+ (5×10^{16} versus 5×10^{12}). Therefore, holes are created predominately via the $(-/0)$ process.



Given the large density of neutral donors still surviving, the next process is the capture of the hole.



This explains why we eventually see for a positive $-U$ in Figure 4-3.

$$N_D^+ = N_D^- \quad . \quad (4-41)$$

These two charge states increase in tandem at the expense of the neutral donor concentration. At the same time, the Fermi level locks halfway between the $(0/+)$ and $(-/0)$ energy level. (At the lowest temperatures,

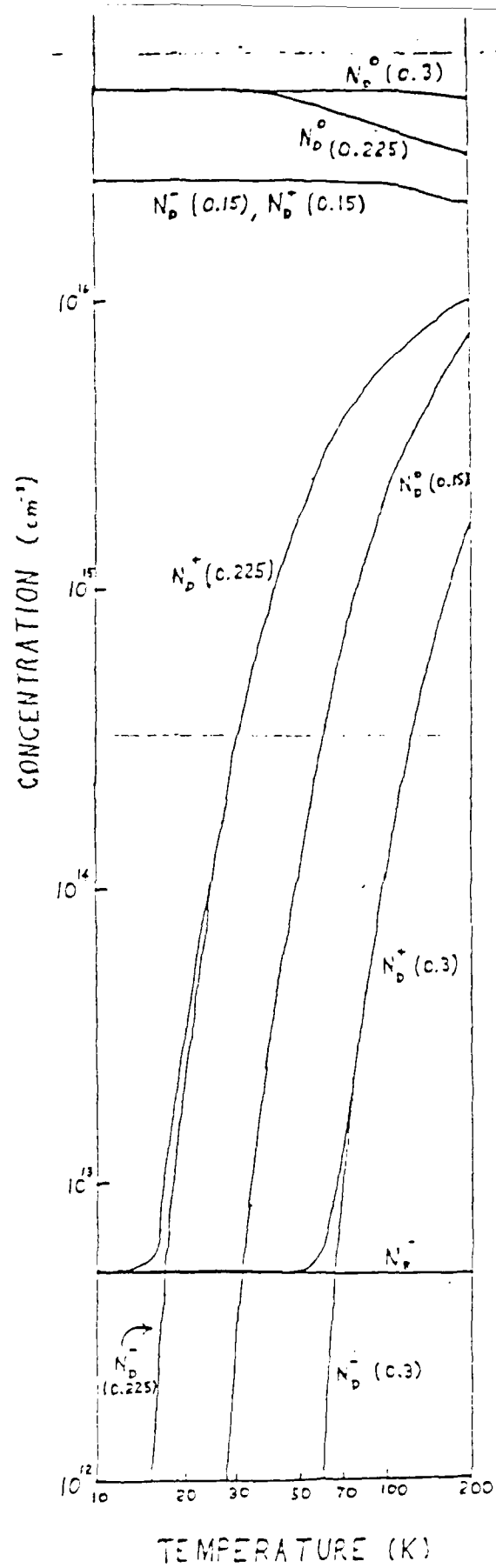


Figure 4-3 Charge Center Concentrations $\phi_B = 0$ $N_B = 5 \times 10^{12}$

the Fermi level is locked at the 0/+ level.) At much higher temperatures than shown in Figure 4-3, the Fermi level is unpinned again, N_D^0 decreases, N_D^- increases, and N_D^+ decreases, while the Fermi level rises.

The behavior of the negative -U center system in Figure 4-3 is exemplified by the 0.15eV (-/0) and 0.20eV (0/+) system. As discussed earlier, the two stable charge configurations are N_D^- and N_D^+ with two and zero electrons, respectively. The introduction of N_D^0 neutral impurities into the crystal, at low temperatures, produces a thermodynamically unstable situation. The system can lower its energy if half the impurities lose an electron and the other half pick one up, i.e.;



(A small fraction of the donors give up one electron to compensate the residual boron.) Thus, in essence, the system is self-compensating.

$$N_D^+ = N_D^- = 1/2 N_D \quad . \quad (4-43)$$

This results in the Fermi level being pinned halfway between the two energy levels

$$\mu = (E_D + E_{DA})/2 \quad . \quad (4-44)$$

As the temperature increases, electrons from the valence band are promoted thermally to the first available empty electronic state (0/+)



since putting another electron on D^- is ruled out (i.e., there is no (=/-) state in the gap).

Some of the D^0 created by the thermal process in Equation 4-45 will spontaneously decay as in Equation 4-42 into D^+ and D^- . The thermal process, Equation 4-45, will lead to an increase in the density of neutral donors at the expense of the N_D^+ concentration.

Another process that leads to an increase of the D^0 population is the hole capture by D^- .



This process is not followed by rapid hole emission to the valence band at low temperature. The processes given in Equations 4-45 and 4-46 produce the increased population of D^0 centers which is seen in Figure 4-3.

For temperature above 200K, which are not shown in Figure 4-3, the hole captured by D^0 in Equation 4-46 will be reemitted to the valence band,



The D^- population will grow, and the D^0 population will decrease. At the same time, there will be a rapid decrease of the D^+ population since the thermal ionization of D^+ leads to



In the second step of this process, D^0 decays via the process of Equation 4-47 which takes less energy than the initial ionization of D^+ . The D^- becomes the more thermodynamically stable charge state at higher temperature because the Fermi level becomes unpinned again and rises above μ given by Equation 4-44. The average number of electrons per donor rises from "one" at low temperatures [$N_D^- = 1/2 N_D$, $N_D^0 = 0$]

$$n_{avg} = (N_D^0 + 2N_D^-) / N_D = (2)(1/2)(N_D / N_D) = 1 \quad (4-49)$$

to two at higher temperatures [$N_D^- = N_D$, $N_D^0 = 0$]

$$n_{avg} = (2)(N_D / N_D) = 2 \quad (4-50)$$

4.8 THERMAL EQUILIBRIUM HIGH BORON CASE

The system in Figure 4-3 for negative $-U$ was self-compensating for lack of a substantial concentration of shallow acceptors. We desire to provide a comparison in Figure 4-4 with the system in Figure 4-3. We now make the density of shallow acceptors (Boron) equal to that of the donors

$$N_B = N_D \quad . \quad (4-51)$$

As the donors enter the silicon matrix, they first compensate the shallow acceptors.



The equal compensation noted in Figure 4-3 means that there are no more electrons available to produce the auto compensation (Equation 4.1); so at low temperatures, we have

$$N_D^+ = N_B^- \quad . \quad (4-53)$$

The Fermi level is now locked half way between the boron level and the $(0/+)$ acceptor level of the donor.

This same fact is true at low temperatures for the positive $-U$ situation in Figure 4-4. The deep donor simply gives up its electron to the shallower boron acceptor and the Fermi level locks halfway in between. As the temperature rises, the conventional process occurs,



D^+ thermally ionizes; this leads to an increase in the D^0 population. As the temperature continues to rise thermal ionization of D^0 occurs,



The final result is an increased population of the D^- .

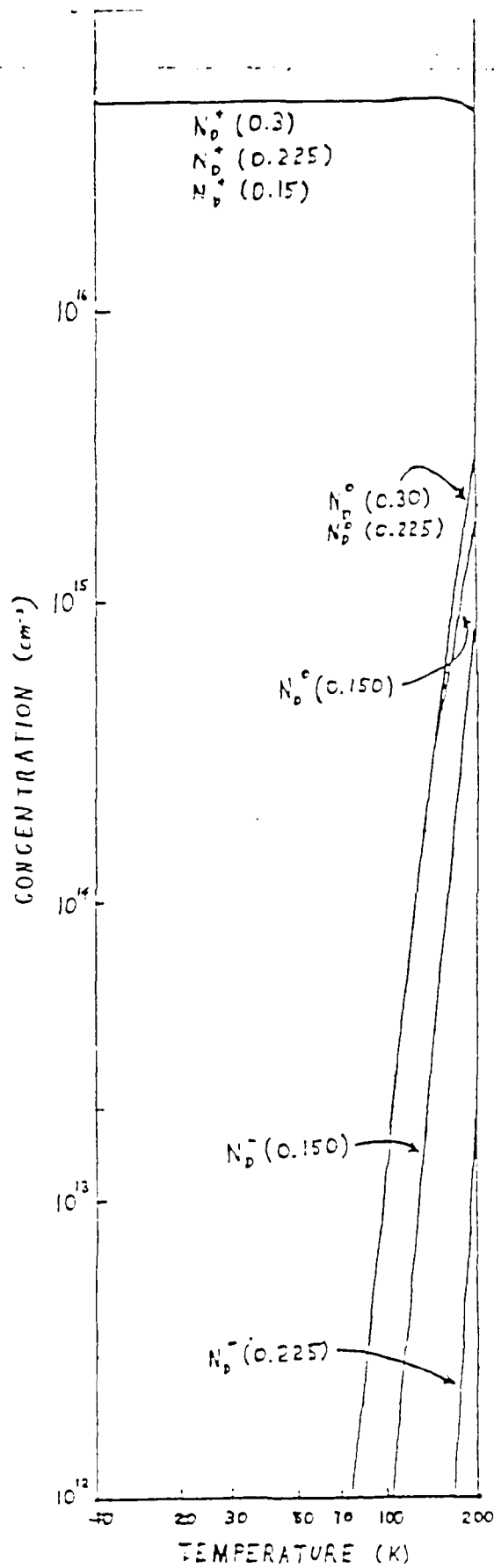


Figure 4-4 Charge Center Concentrations $N_B = N_D$

The average number of electrons per donor increases from zero at low temperatures, as the Fermi level rises, to a plateau of one electron per donor as the Fermi level passes the (0/+) level. The average number of electrons reaches a value of two per donor when the Fermi level rises above the (-/0) level.

The temperature behavior of the negative -U system in Figure 4-4 differs substantially from that of the positive -U system. The first step is to thermally ionize the (0/+) level



This is similar to the case for the positive -U system in Figure 4-4 (Equation 4-54). The difference is in the subsequent fate of some of the neutral donors. The next transition from D^0 to D^- is less likely to occur in the positive -U system than in the negative -U system at the temperature where D^+ is easily ionized to become D^0 . As a matter of fact, once the transition in Equation 4-56 is accomplished in the negative -U system, the next transition required even less energy



This explains why the D^- population grows faster and the D^0 population slower in the negative -U system. The average number of electrons per donor atom increases rapidly from 0 to 2, without a plateau at one electron per donor, as the Fermi level rises with temperature.

4.9 BACKGROUND ILLUMINATED CASE

An understanding of carrier dynamics is necessary to explain the detector performance described in the next section. In a typical high background application, the background flux is

$$\Phi_B = 1 \text{ E } 16 \text{ photons/cm}^2\text{-sec}$$

The carriers dynamics is explored using the same equations as before, but with optical generation included. Figures 4-5 and 4-6 detail the behavior of the low and high counterdoped systems, respectively.

4.9.1 Low Boron, with Illumination

The presence of the substantial photon flux produces a large redistribution of charge. The positive -U system behavior may be analyzed as follows. Essentially all donors are neutral for the low temperature - no light case in Figure 4-3.

$$N_D^0 = N_D$$

When the light is turned on, the following transition occurs



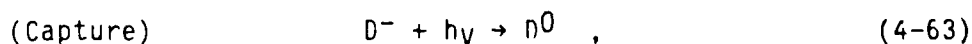
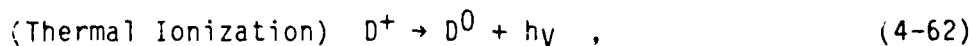
Simple capture of the carrier produces



The capture process by the neutral donor (Equation 4-59) is made likely owing to the large concentration of neutral donors; this is in spite of the low recombination cross-section, Table 4-1. The system is self compensating in the presence of light

$$N_D^+ = N_D^- \quad (4-61)$$

As the temperature increases, the behavior of the positive -U system depends on the relative positions of the two energy levels. It is easier to reverse the process in Equations 4-58, 4-59, and 4-60 (produce neutral donors) for the deeper center $E_{DA} = 0.3$,



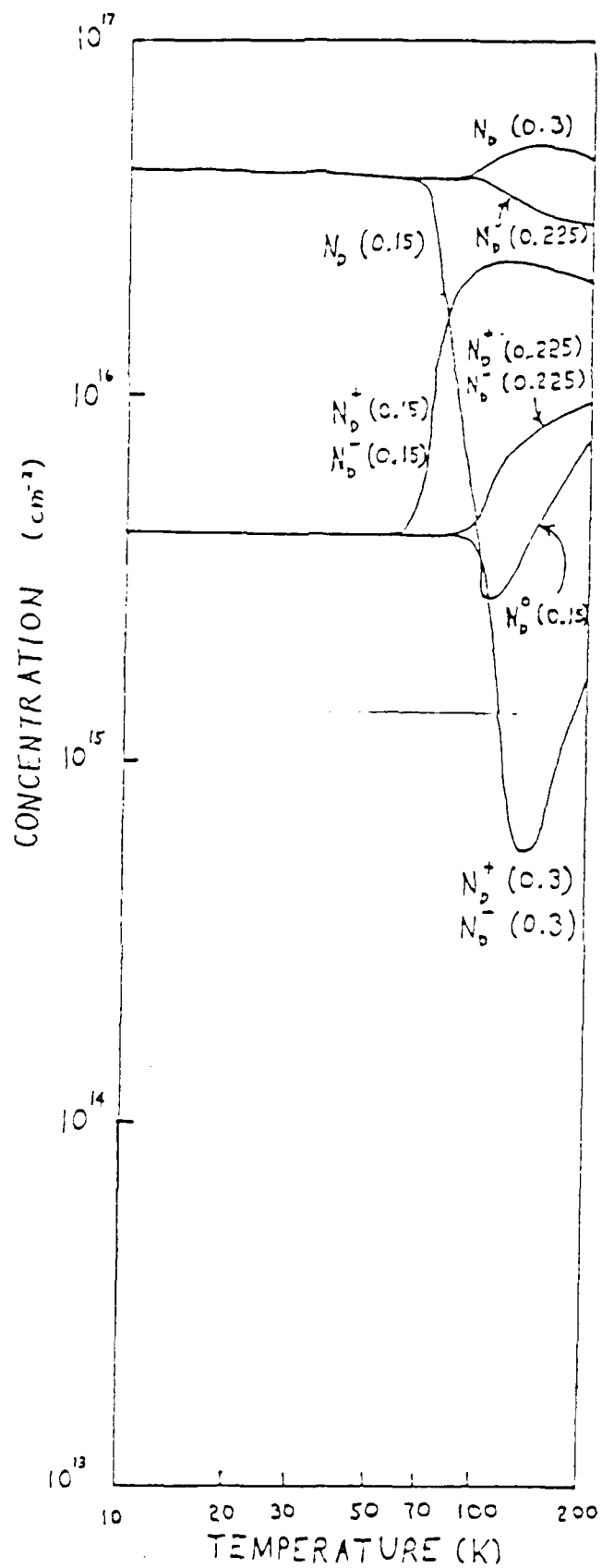


Figure 4-5 Low Counterdoped Systems

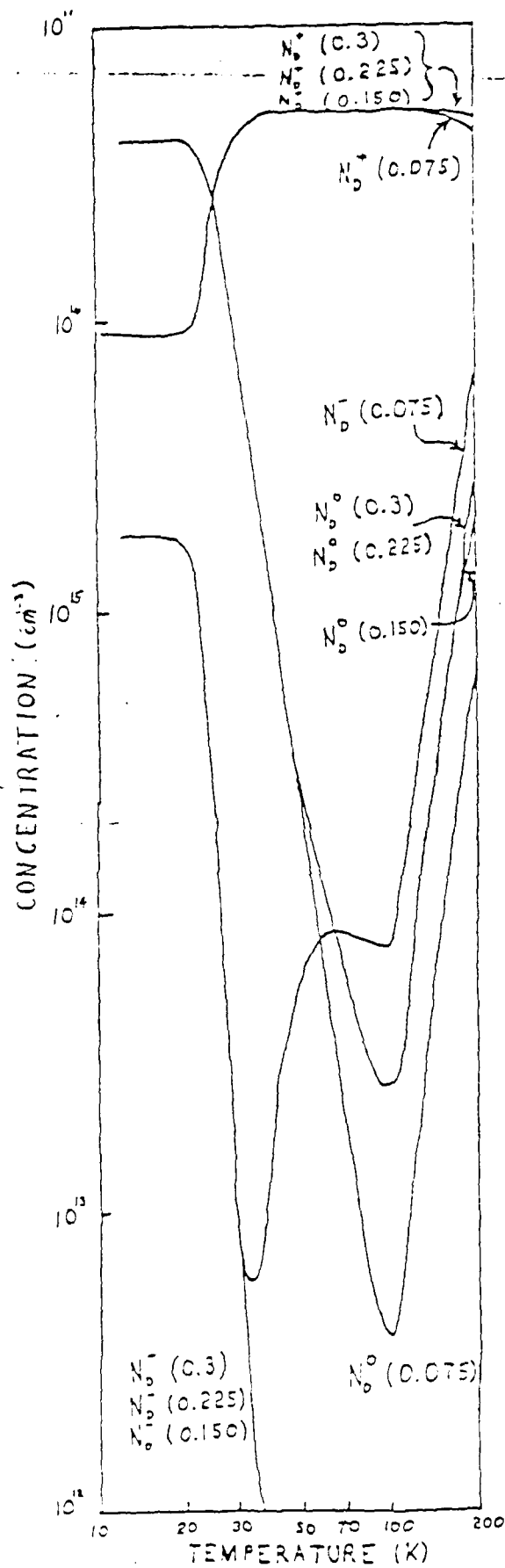


Figure 4-6 High Counterdoped Systems

than to produce further thermal ionization of D^0



This leads to the increase of N_D^0 and the decrease of N_D^+ and N_D^- . At still higher temperatures, the thermal ionization of D^0 becomes likely (Equation 4-64) as is the capture of a hole.



So that N_D^+ and N_D^- increase, and N_D^0 decreases.

When $E_{DA} = 0.225$, it is easy to thermally ionize D^0 (Equation 4-64), since $E_{DA} \sim E_D$ in this parametric model. This is followed by the capture process (Equation 4-65). Therefore, N_D^+ and N_D^- increase at the expense of N_D^0 .

The explanation for the behavior of the negative -U system is as follows. We have at low temperatures in thermal equilibrium

$$N_D^+ = N_D^- = 1/2 N_D \quad , \quad (4-66)$$

optical absorption leads to



while there are no allowed transitions of the form



What happens though is that some of the newly created neutral donors decay spontaneously via



and the system is self-compensating again. The overall effect of background light at low temperatures is the production of an otherwise metastable N_D^0 population at the expense of N_D^+ and N_D^- .

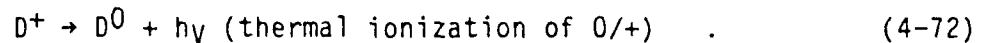
As the temperature increases, the N_D^0 population is thermally ionized.



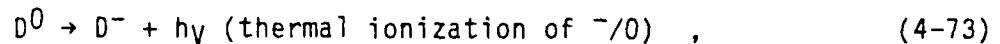
and a hole is captured



At still higher temperatures the (0/+) level comes into the picture and the reverse of Equations 4-70 and 4-71 occurs,



and



This replenishes the D^0 population at the expense of the D^+ . In Figure 4-5, the self-compensation is the necessary consequence of the very low boron concentration and low hole concentration in the temperature regime of interest.

4.9.2. High Boron, with Illumination

For high counterdopant concentration, the thermal equilibrium situation is depicted in Figure 4-4. Essentially all the donors are used up to compensate boron

$$N_D^+ = N_D \quad . \quad (4-74)$$

As the light is turned on, there will be the photoionization process



followed by



This produces a substantial N_D^0 , N_D^- density. Most holes thus produced are captured by N_B^- rendering most boron neutral.

Next, we discuss the positive $-U$ system as the temperature increases, neutral boron begins to emit holes to the valence band. Those holes that are recaptured by boron are even faster reemitted to the valence band. Therefore, capture at the boron atoms becomes unlikely as the temperature increases. The capture of these holes by D^0 and D^- is more likely.



which will lead to a decrease of the D^- and D^+ concentrations. At still higher temperatures, the thermal ionization of the $(0/+)$ level produces a hole.



This results in a decrease of N_D^+ and an increase in N_D^0 .

The negative $-U$ systems in Figure 4-6 behave similarly for $E_{DA} = 0.150\text{eV}$ and $E_{DA} = 0.075\text{eV}$. The original populations of the charge states are the same for the positive and negative $-U$ systems at low temperatures and in the absence of light (Figure 4-4). The photoionization of the D^+ (Equation 4-75 and 4-76) and the hole capture by N_B^- shift the compensation from boron when the background flux is on. Large concentrations of D^0 ; D^- and neutral boron are created. As before, with increasing temperature it is the turn of boron to emit holes to the valence band. These holes are captured by D^0 and D^- , (Equations 4-77 and 4-78) as in the case of the positive $-U$ system in

Figure 4-6. The $E_{DA} = 0.075\text{eV}$ system shows that with a further increase of temperature the $(-/0)$ level participates in the thermal ionization



This produces an increase in N_D^- and a decrease in N_D^0 .

A further increase in temperature involves the $(0/+)$ level in the conversion D^+ to D^0 which thus increases N_D^0 at the expense of N_D^+ .



Of course, some of the D^0 will be converted to D^- (Equation 4-80) since $E_{DA} < E_D$. This is the main difference between the positive and negative $-U$ systems in Figure 4-6.

4.10 RESPONSIVITY

Responsivity (Equation 4-36) is a measure of the detector's ability to detect incident signal radiation while the detector is at temperature "T" and is already exposed to the background radiation. The partial derivative in Equation 4-36 measures the additional photohole density Δp when additional flux " $\Delta\phi$ " falls on the detector.

Figure 4-7 displays the calculated responsivities for several systems of interest. The behavior of responsivity is easily understood in the high temperature region $T > 100\text{ K}$. We recall that the principal photoconductive transition is given by



This results in high quantum efficiencies and responsivities being promoted by large D^+ concentrations. Figure 4-6, for high dopant concentrations, shows that N_D^+ increases with temperature as the

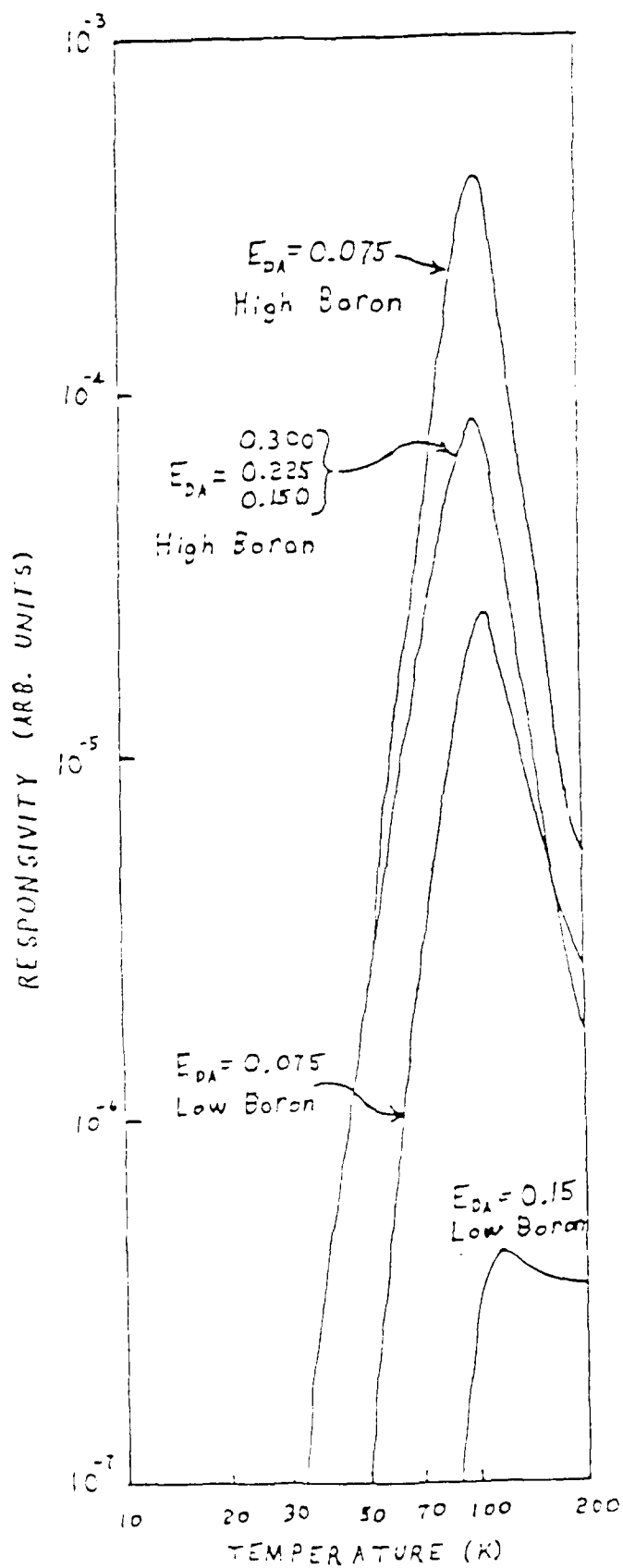
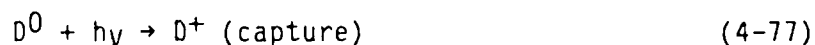


Figure 4-7 Calculated Responsivity

compensation is shifted back to boron. This makes the material more sensitive to the incoming radiations, which means it is more responsive. The D^+ are thermally ionized above 100K; this produces N_D^0 and results in a drop in responsivity.

The negative -U system $E_{DA} = 0.075\text{eV}$ has about five times as high a responsivity as the systems with $E_{DA} \geq 0.15$. This, the most negative -U system considered in this work, has a more efficient transfer of holes from boron to D^0 (Equation 4-77),



It also is most efficient in thermal emission of holes by D^0 because E_{DA} is small.



Capture of the hole is the next step. This gives rise to an enhanced D^+ population which is responsible for the large responsivity.

The counterdoping concept, with the large boron concentration, works because donors compensate boron. Thus the desired deep donor level is exposed. This works for both the positive and negative -U systems. What is not appreciated is that the counterdoping scheme works without any boron if the center has the negative -U property. As discussed in connection with Figures 4-3 and 4-5, for low boron concentrations, the system is self-compensating. The responsivity for the $E_{DA} = 0.075\text{eV}$ ($N_B = 5 \times 10^{12} \text{ cm}^{-3}$) system in Figure 4-7 is within an order of magnitude of the high boron case. This disadvantage may be offset by what is expected to be the larger hole mobility in the boron free negative -U system.

4.11 DETECTIVITY

The thermal generation-recombination (G-R) noise limits the detectivity of photoconductive infrared detectors. Detectivity is therefore degraded when there is a large scale thermal emission of holes

to the valence band. The detector is background-limited, at low temperatures, when the only aperture noise mechanism is the background photon induced generation-recombination noise (Figure 4-8). The detectivity is then temperature independent. The first temperature roll-off in the detectivity occurs when boron is thermally ionized for the high boron case. The large increase in the hole population gives rise to the G-R noise. These holes are subsequently recaptured by the donors and the detectivity flattens out. At higher temperatures, the emission of holes from the (0/+) donor level produces the final temperature roll-off for $T > 100\text{K}$.

The low boron case, $E_{DA} = 0.075\text{eV}$, negative $-U$ case, shows the first roll-off at higher temperature than the high boron case $E_A = 0.044\text{eV}$. Here, the first thermal roll-off is due to the hole emission by the neutral donors with the E_{DA} activation energy. All the systems compared in Figure 4-8 show comparable detectivities.

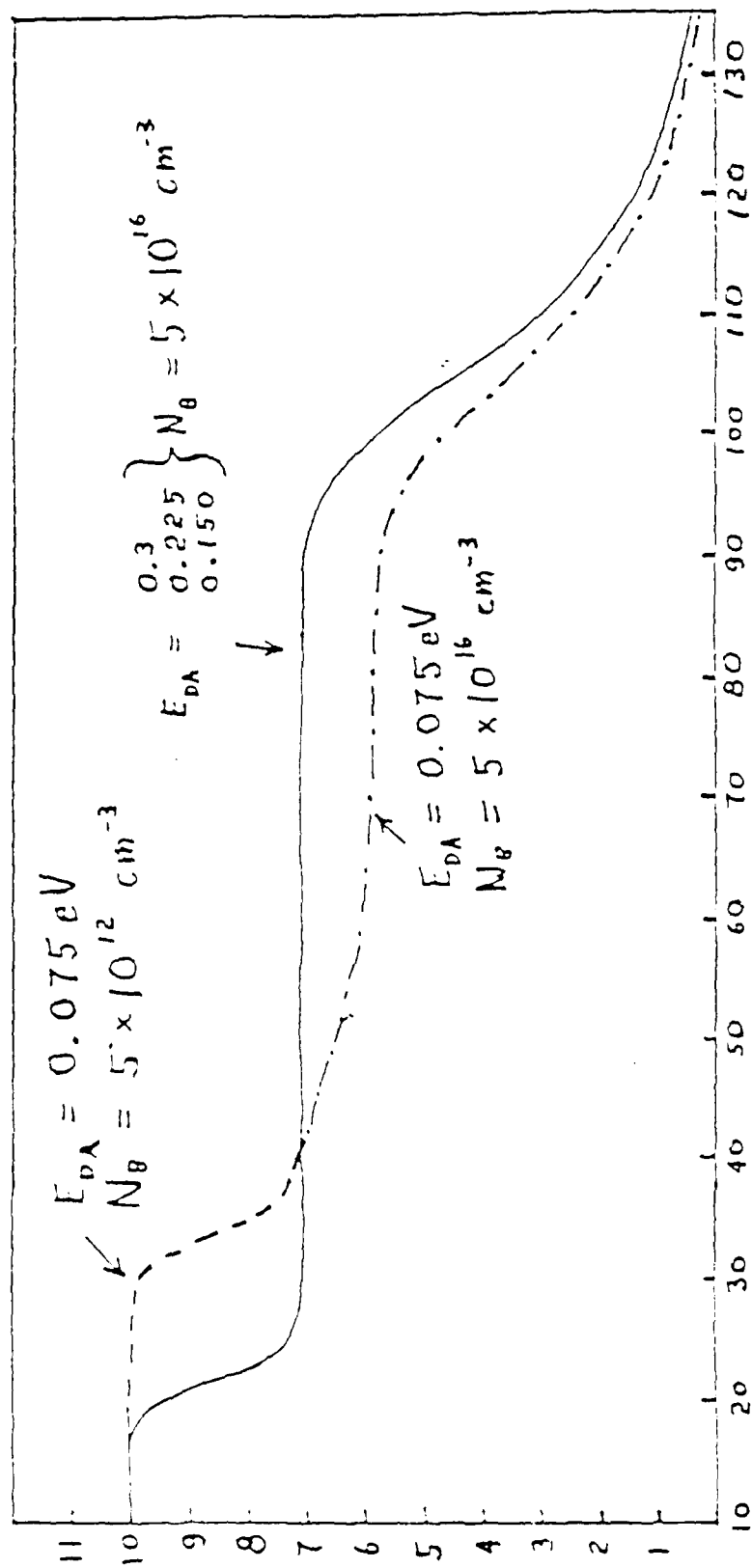


Figure 4-8 Detectivity vs. Temperature

5.0 CONCLUSIONS

The counterdoping scheme has been modeled for systems exhibiting multivalent statistics. Interesting differences were observed for systems with negative and positive $-U$ properties. This may well be the first such investigation of the infrared detector potential of the negative $-U$ center and of the multivalent statistics in the counterdoped scheme.

We find that positive and negative $-U$ systems show similar detectivities and T_{BLIP} temperatures. Most interesting, for detector applications, is that the negative $-U$ systems are self-compensating, or self-counterdoped, because of the inverted level ordering. They appear to have comparable responsivities to that of the boron counterdoped detectors. More quantitative predictions await better experimental input to the theory.

The model outlined in the theoretical section has identified the relevant parameters which control the operating temperature and figure of merit for the counterdoped detector. The rate equation can be used to predict the response of any counterdoped system. In particular, it can be used to optimize doping concentrations for the highest BLIP operating temperature.

We have successfully created the positive divacancy and observed to presence using DLTS, Hall and infrared analysis. The presence of boron and carbon in the silicon sample lead to creation of other complexes which were also observed. These are the interstitial carbon - substitutional carbon trap at $E_v + 0.44\text{eV}$ which was observed in the DLTS spectra [Section 3.1 and 3.2] as well as the boron related trap which closely overlaps the positive divacancy.

The final statement is that the evidence produced in the infrared spectral measurements shows that illumination does not upset the creation of positive divacancies. The counterdoping concept is valid in that boron compensation serves to create positive divacancies and prevents formation of neutral and negative divacancies.

ACKNOWLEDGEMENTS

Many people have contributed to the technical success of this program. I provide a listing of their names to serve as an indication that a research program is a large undertaking.

Gail Brown who patiently waited for us to start work.

Richard Engel for float zoning the silicon ingots.

Joe Hemskey for taking his own time to electron irradiate the slices.

Alan Smith who made the Schottky diodes on the evaporator.

Ed Jaworowski for DLTS analysis.

Jim Robison for DLTS analysis.

Steve Smith for DLTS analysis.

Frank Szmulowicz and his theoretical analyses.

Dave Fischer who provided the infrared absorption spectra.

Tim Peterson and his Hall measurement data.

Lisa Beljan for producing this report.

REFERENCES

- [1-1] C.T. Elliott, P. Migliorato, and A.W. Veri "Counterdoped Extrinsic Silicon Infrared Detectors," *Infrared Physics* 18 65 (1978).
- [1-2] R. Bauerlein, "Radiation Damage in Solids."
- [2-1] D.V. Lang, *J. Appl. Phys.* 45, 3022 (1974).
- [2-2] D.V. Lang, L.C. Kimerling, *Proc. Intern. Conf. Lattice Defects in Semiconductors, Freiberg 1974* (Inst. Phys. Conf. Series No. 23, London 1975) p. 581
- [2-3] D.V. Lang, in "Thermally Stimulated Relaxation in Solids" ed. P. Braunlich (Springer-Verlag Berlin Heidelberg New York 1979) p. 33.
- [3-1] K.L. Brower, *Phys. Rev. B* 9, 2607 (1971).
- [3-1-1] C.A. Londos, *T. Phys. Chem. Solids*, Vol. 47, No. 12 1g. 86, pgs. 1147-1151
- [3-2] A.E. Jaworowski, C.B. Pierce, S. Burdick, J.W. Corbett and J.I. Hanoka, *J. Appl. Phys.* 52, 2337 (1981).
- [3-3] L.C. Kimerling, *IEEE Trans. Nuclear Sci.* 23, 1497 (1976).
- [3-4] G.D. Watkins and J.W. Corbett, *Phys. Rev.* 138, A543 (1965).
- [3-5] P.M. Mooney, L.J. Cheng, M. Suli, J.D. Gerson, and J.W. Corbett *Phys. Rev. B* 15, 3836 (1977).
- [3-6] A. Chantre, *Phys. Rev. B* 32, 3687 (1985).
- [3-7] P.J. Drevinsky and H.M. DeAngelis, *J. Electron Mater.* 14a, 815 (1985).
- [3-8] C.A. Londos, *J. Phys. Chem. Solids*, 47, 1147 (1986).
- [3-9] C.A. Londos and P.C. Banbury, *J. Phys. C: Solid State Phys.* 20, 645 (1987).
- [3-10] L.W. Song, B.W. Benson, and G.D. Watkins, *Phys. Rev. B* 33, 1452 (1986).
- [4-1] F. Carton - Merlet et al, *J. Phys. C* 15 2339 (1982).
- [4-2] Frank Szmulowicz, "Parametric Study of a Silicon Counterdoped Detector System", *Proc. IRIS Conference on Detector Materials*, Menlo Park, CA (June 1986).

- [4-3]W. Shockley and J. T. Last, Phys. Rev. 107 392 (1957).
- [4-4]J. S. Blakemore, Semiconductor Statistics, (MacMillian, New York 1962.)
- [4-5]David C. Look in Semiconductors and Semimetals, edited by R.K. Willardson and Albert C. Beer (Academic Press N.Y. 1983) Vol. 19, pgs. 75-170.
- [4-6]G. A. Baraff, E.O. Kane and M. Schliiter, Phys. Rev. B21 (1980).
- [4-7]G. D. Watkins and J. R. Troxell, Phys. Rev. Lett. 44 593 (1980).
- [4-8]J. R. Troxell and G. D. Watkins, Phys. Rev. B22 921 (1980).
- [4-9]H. J. Hoffman, Phys. Rev. Lett. 45 1733 (1980).
- [4-10]D. C. Look, Phys. Rev. B24, 5852 (1981).
- [4-11]L. I. Shpinar and I. I. Yaskovets, Sov. Phys. Semicond. 19, 1135 (1986).
- [4-12]G. D. Watkins and J. W. Corbett, Phys. Rev. 138A, 543 (1965); Phys. Rev. 138A, 555 (1965).
- [4-13]R. G. Humphreys, S. Brandt and M. Jaros, J. Phys. C16 L337 (1983).
- [4-14]S. T. Pantebiles, I. Ivanor, M. Scheffler and J. P. Vigneron, Proc. 12th Int. Conf. on Defects in Semiconductors, Amsterdam (1983).
- [4-15]Frank Szmulowicz, Patrick Hemenger, and Shaun McGuigan Proc. Materials IRIS Conference Colorado Springs, CO 1985.

APPENDIX

PARAMETRIC STUDY OF A SILICON
COUNTERDOPED DETECTOR SYSTEM

10 June 1986

Frank Szmulowicz*
University of Dayton Research Institute
Dayton, Ohio 45469

ABSTRACT

A parametric study of a counterdoped extrinsic silicon detector system is presented. The system consists of a shallow group III acceptor and a deep donor with a level near the valence band. It is known that compensated donors become neutral upon photoabsorption and present a very small capture cross section for the carriers. This leads to a higher BLIP operating temperature for the counterdoped system than for the conventional detector operating at the same wavelength. A detailed microscopic model for the counterdoped system is developed to study the temperature dependence of responsivity and detectivity. Detectivity is studied as a function of the hole-neutral donor recombination coefficient and as a function of the acceptor-to-donor density ratio. The best detectivities and, simultaneously, responsivities are obtained for acceptor density equal to that of the donors. Using boron, aluminum, gallium, or indium as the group III acceptor in the parametric study shows that the highest responsivities and detectivities are obtained for the shallowest acceptor, that is, boron. These results can be understood on the basis of the picture involving optical and thermal carrier generation, carrier recombination, and the dynamic interaction of the donor and acceptor levels mediated by the valence band.

1.0 INTRODUCTION

Extrinsic silicon infrared detectors in the 3-5 μm range are limited to operating temperatures lower than 60K. High BLIP (Background Limited Infrared Photoconductor) temperature silicon infrared detectors are required to reduce the size and weight of the cooling systems associated with the detector arrays. The limitation on the detector operating temperature can be traced to the large recombination coefficients of carriers in conventionally doped extrinsic silicon.

A scheme for increasing the BLIP operating temperature of an extrinsic detector has been proposed by Elliott, Migliorato, and Vere¹. Specifically, they proposed to dope a semiconductor with either a deep donor or a deep acceptor and then counterdope the material with impurity of opposite kind. The principal IR-active centers are the deep impurities which have lost charge to the compensating

* This work is supported by the Materials Laboratory, Air Force Wright Aeronautical Laboratories, Contract No. F33615-85-C-5062.

¹ Elliott, C. T., Migliorato, P., and Vere, A. W., "Counterdoped extrinsic silicon infrared detectors," *Infrared Physics* 18, 65 (1978).

counterdopant. Therefore, the deep acceptors become negatively charged and deep donors become positively charged.

In the conventionally doped extrinsic detectors IR excitation produces photocarriers of one sign and an immobile center of opposite sign. The attractive interaction between the carriers and the photoionized centers leads to short carrier lifetimes which ultimately results in low detector operating temperatures. On the other hand, in the counterdoped detector the photoionized center becomes neutralized in the photoabsorption and can be either neutral or even repulsive to the created photocarriers. As the result the recombination coefficients are decreased and carrier lifetimes are increased, which leads to higher BLIP operating temperatures.

The original proposal of Elliott, Migliorato, and Vere contains a theoretical analysis of the counterdoped system. In particular, these authors provided expressions for spectral responsivities and detectivities as well as for the BLIP temperature. The present work will provide a more detailed microscopic model of the counterdoped system and will explore the detector performance parameters over the whole temperature range. By examining the carrier dynamics as a function of doping conditions and recombination coefficients, specific recommendations can be made for optimum choice of detector parameters. It is hoped that the present model will add to the understanding of the physical basis for the counterdoped detector.

Section 2 describes the model of the counterdoped system, while Section 3 is devoted to the presentation of results. Section 4 contains the principal conclusions of this work.

2.0 MODEL OF THE COUNTERDOPED SYSTEM

2.1 DESCRIPTION OF THE DETECTOR

Figure 1 displays the schematic band diagram for the counterdoped semiconductor. The principal infrared active dopant is the deep donor with energy level in the gap at energy E_D from the valence band. The donor concentration is N_D . For the sake of simplicity, the center responsible for the donor formation can only be either neutral or singly positively charged. Extension of the present formalism to multivalent flaws or impurities should be straightforward.

The system is also doped with acceptors with density N_A at energy E_A above the valence band corresponding to the 0/- charge transition of the center. The simplest and in practice best realization of the acceptors are the simple hydrogenic column III impurities: boron, aluminum, gallium, or indium. At low temperatures donors lose one electron each to the acceptors below so that

$$N_D^+ = N_D = N_A^- \quad \text{for } N_D \leq N_A \quad (1)$$

or

$$N_D^+ = N_A = N_A^- \quad \text{for } N_D \geq N_A \quad (2)$$

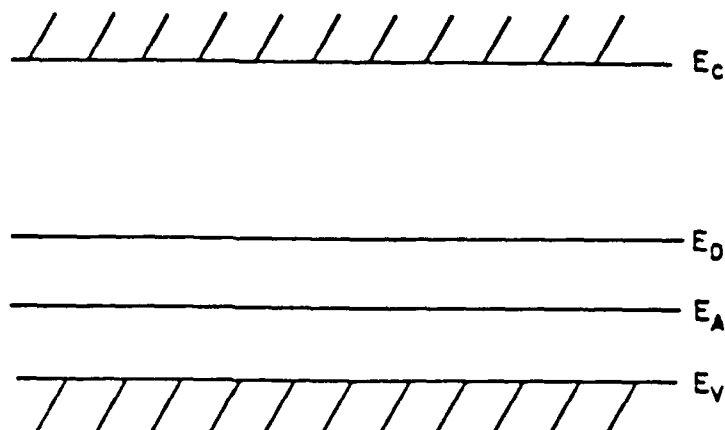
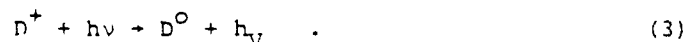


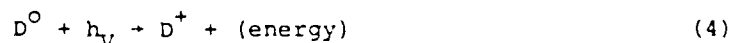
Figure 1. Schematic energy level system for the counterdoped system containing a shallow acceptor and a deep donor level. E_C , E_V , E_D , and E_A stand for the conduction band, valence band, the donor level, and acceptor level energy positions, respectively.

Photoconductivity results from photoabsorption of a photon with energy $h\nu \geq E_D$, by a valence electron which is then promoted to the donor level



As the result the donor is neutralized and a hole in the valence band, $h\nu_V$, is created. The photocurrent is carried by the valence band holes. Equivalently, of course, one may think of Eq. (3) as a promotion of the hole on the donor level, D^+ , to the valence band.

The hole lifetime in the valence band, as the hole is swept out by the electric field in the detector, ought to be long since the recombination cross section for the hole capture by neutral acceptors should be very small. The recombination process would proceed via the reaction



which has to be contrasted with the recombination process in the standard p-type photoconductive detector where



In Eq. (5) the recombination cross section for the hole capture by the attractive center is estimated to be several orders of magnitude larger than for the process, Eq. (4), in the counterdoped detectors. For multivalent flaws it is possible to have the capturing center to be of the same electrical sign as the photocarrier, which would further reduce the recombination cross section.

In order to calculate the two figures-of-merit for the photodetector, the responsivity and detectivity, the rate equations for the optical and thermal carrier generation must be solved². The rate at which neutral acceptors are produced is given by

²Szmulowicz, Frank, Hemenger, Patrick, and McGuigan, Shaun, "Low background performance modeling of gallium doped silicon infrared detectors," Proc. Materials IRIS Conference, Colorado Springs, CO (1985).

$$\frac{\partial N_A^O}{\partial t} = p B_A N_A^- - N_A^O \langle \sigma_A \phi \rangle - N_A^O \frac{B_A}{g_A} N_V \exp(-E_A/k_B T) \quad (6)$$

where

- g_A = the degeneracy of the acceptor level, $g_A=4$
- B_A = the recombination coefficients for holes with the ionized acceptor, Eq. 5
- p = valence band hole concentration
- N_A, N_A^O, N_A^- = total acceptor, neutral acceptor, and ionized acceptor concentrations, respectively
- σ_A = wavelength dependent photoabsorption cross section for the acceptor level
- ϕ = incident photon flux consisting of the background, ϕ_B , and signal, ϕ_S , radiation
- $\langle \sigma_A \phi \rangle$ = convolution of the photon flux with the photoabsorption cross section
- N_V = effective valence band density of states
- E_A = acceptor photoionization energy.

The convolution $\langle \sigma \phi \rangle$ will be replaced by $\sigma_p \phi$, where σ_p is the peak photoabsorption cross section for the given impurity. The replacement thus defines an effective flux ϕ .

The first term in Eq. (6) represents the hole capture rate by ionized acceptors. In the present parametric study, B_A will be taken to be $E_A=6 \times 10^{-4}/T^{1.5}$ (cm^3/sec). The temperature dependence of B is consistent with the results of Geim, Pensl, and Schultz³ on indium and gallium in silicon and with the theoretical model of Lax⁴. The numerical prefactor is also typical of the results of Geim et al. The second term in Eq. (6) gives the photoabsorption rates of holes from neutral acceptors and the third term gives the corresponding thermal hole generation rate. The typical peak photoabsorption cross section for simple acceptors in silicon is in the $\sigma_A=10^{-15}$ - 10^{-16}cm^2 range. Given that in steady state $\partial N_A/\partial t = 0$, and

$$N_A = N_A^O + N_A^- \quad (7)$$

gives

$$N_A^- = \frac{\sigma_A N_A}{p + \sigma_A} \quad (8)$$

where

$$\sigma_A = (N_V/g_A) \exp(-E_A/k_B T) + \langle \sigma_A \phi \rangle / B_A \quad (9)$$

For donors the rate equation is given by

$$\frac{\partial N_D^+}{\partial t} = B_D p N_D^O - g_D B_D N_V \exp(-E_D/k_B T) N_D^+ - N_D^+ \langle \sigma_D \phi \rangle \quad (10)$$

where

- N_D, N_D^O, N_D^+ = total, neutral, and ionized donor densities
- B_D = the recombination coefficient for holes with neutral donors (to be varied in the calculation)

³Geim, K., Pensl, G., and Schultz, M., "Shallow acceptor population and free hole concentration in Si:In and Si:Ga with IR-photoexcitation," Appl. Phys. **A27**, 71 (1982).

⁴Lax, M., "Cascade capture of electrons in solids," Phys. Rev. **119**, 1502 (1960).

- g_D = the degeneracy factor for the donor level, taken to be $g_D=2$ for the sake of concreteness
 E_D = the donor level position with respect to the valence band
 σ_D = the photoabsorption cross section of the ionized donor level, Eq. (3).

Please note the different placement of the degeneracy factors in Eqs. (6) and (10). These can be shown to be necessitated by the detailed balance conditions. The first term in Eq. (10) is the hole capture rate by neutral donors, the second and third are the thermal and optical excitation rates of holes to the valence band from the ionized donors, Eq. (3). Again, in the steady state $\partial N_D^+ / \partial t = 0$, and since

$$N_D = N_D^0 + N_D^+ , \quad (11)$$

Eq. (10) yields

$$N_D^+ = \frac{N_D^0 p}{a_D + p} , \quad (12)$$

where

$$a_D = N_V g_D \exp(-E_D/k_B T) + \langle \sigma_D \phi \rangle / B_D . \quad (13)$$

Using the charge neutrality condition

$$N_D^+ + p = N_A^- , \quad (14)$$

together with Eqs. (8) and (12), result in the cubic equation for p ,

$$p^3 + p^2 [N_D + a_A + a_D] + p a_A [a_D + N_D - N_A] - N_A a_A a_D = 0 . \quad (15)$$

Equation (15) has to be solved for p at different temperatures and background flux levels. In special circumstances Eq. (15) reduces to an easily solvable quadratic or even a linear equation. In general, though, one must solve the cubic equation.

2.2 DETECTOR PERFORMANCE MODEL

Spectral responsivity is defined as the signal current per unit incident signal radiation power. The signal current is proportional to the density of signal generated carriers p_s which is the difference between the densities of holes with and without the signal flux on, i.e.

$$p_s = p(\phi_B + \phi_s, T) - p(\phi_B, T) . \quad (16)$$

In the small signal approximation we can take, from Eq. (16), the signal flux generated carrier density to be

$$p_s \sim (\partial p / \partial \phi) \phi_B \phi_s . \quad (17)$$

Since the signal power is also proportional to ϕ_s , the responsivity is proportional to

$$R \sim (\partial p / \partial \phi) \phi_B \quad (18)$$

with the derivative evaluated at $\phi = \phi_B$.

The spectral detectivity is proportional to the ratio of the responsivity to the root-mean square noise current

$$D^* \sim R / I_n . \quad (19)$$

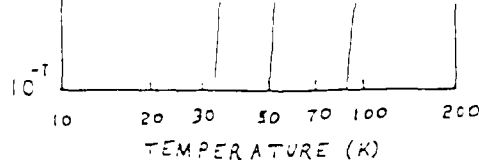


Figure 4-7 Calculated Responsivity

The generation-recombination noise current is given by

$$I_N = (4I_0 e G \Delta f)^{1/2}, \quad (20)$$

where I_0 is the background photon and thermally generated current

$$I_0 \sim p(\phi_B, T),$$

Δf is the bandwidth of the measuring electronic circuit, and G is the gain of the detector. The gain is the ratio of the number of holes per second flowing through the detector per photon absorbed in it, i.e.,

$$G \sim I_S / \phi_S. \quad (21)$$

Since $I_S \sim p_S (\partial p / \partial \phi)_B \phi_S$, from Eq. (17), the gain becomes

$$G \sim (\partial p / \partial \phi)_B. \quad (22)$$

Altogether, Eqs. (20-22) give

$$p^* \sim \sqrt{\frac{(\partial p / \partial \phi)_B \phi_B}{p}}. \quad (23)$$

Eqs. (18) and (23) constitute the primary means for evaluating the two figures of merit for the detector. In the present parametric study it is less important to display absolute magnitudes of the performance figures than it is to compare the performance of detectors as various detector parameters are varied.

The hole density p in Eq. (23) is calculated from the cubic equation, Eq. (15). The derivative of p with respect to the photon flux is given by

$$\left(\frac{\partial p}{\partial \phi} \right)_{\phi_B} = \frac{\frac{N_D p}{(a_D + p)^2} \frac{\partial a_D}{\partial \phi} + \frac{N_A p}{(a_A + p)^2} \frac{\partial a_A}{\partial \phi}}{1 + \frac{N_D a_D}{(a_D + p)^2} + \frac{N_A a_A}{(a_A + p)^2}}, \quad (24)$$

which is symmetric in A, D indices.

3.0 RESULTS

Figure 2 shows the calculated detectivity for the input parameters of Table 1. Note that the donor level has been placed arbitrarily at the energy of gallium acceptor in silicon, with the donor concentration and its absorption cross section also typical of gallium. Therefore, Figure 2 can also be used to compare a counterdoped and a conventional detector operating in the same wavelength range. In Figure 2 the compensation is exact $N_A = N_D$ and the recombination coefficient is varied over six orders of magnitude from that typical of attractive centers in conventionally doped detectors to the small recombination coefficients expected of neutral or repulsive centers in counterdoped detectors. Using the input in Table 1, Figure 2 indicates the possibility of raising T_{BLIP} from about 25K to 55K for the detector operating in the 8-13 μ m window. I hasten to add that at present there is no suitable deep donor in this wavelength range.

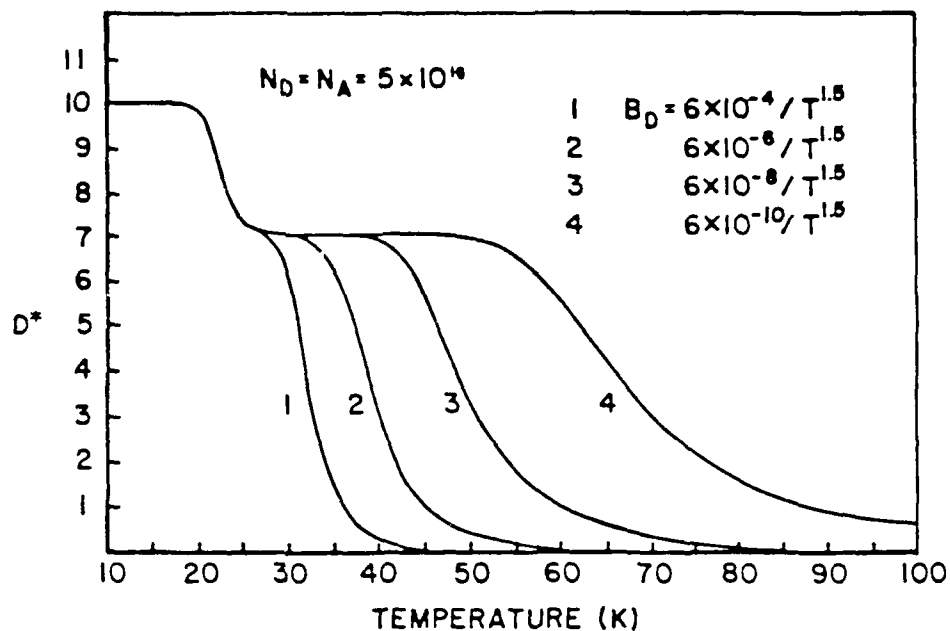


Figure 2. The detectivity of a model counterdoped system as a function of the recombination coefficient and temperature. The detectivity is displayed on a relative scale.

Table 1. Input parameters for the results of the calculation displayed in Figures 2, 3, and 4. The background level is taken to be $\phi_B = 10^{16}$ photons/cm²-sec.

	Donors	Acceptors
g	2	4
σ (cm ²)	5.4×10^{-16}	1.8×10^{-15}
B (cm ³ /sec)	Variable	$6 \times 10^{-4} / T^{1.5}$
concentration (cm ⁻³)	5×10^{16}	5×10^{16}
energy (meV)	72	45

The choice of exact compensation for the display in Figure 2 and the shape of the detectivity curve has to be explained. In Figure 3 B_D is fixed at $6 \times 10^{-10} / T^{1.5}$ (cm³/sec) and N_D at 5×10^{16} cm⁻³, while the acceptor compensating density is varied. The choice of the N_A/N_D ratio will have to be deferred until corresponding responsivity curves, Figure 4, are discussed.

Let us begin the discussion of Figure 3 with the $N_A = N_D$ case. At the lower of temperatures, without the background flux, all the donors and acceptors are ionized;

$$N_A^- = N_A, \quad N_D^+ = N_D, \quad p = 0. \quad (2)$$

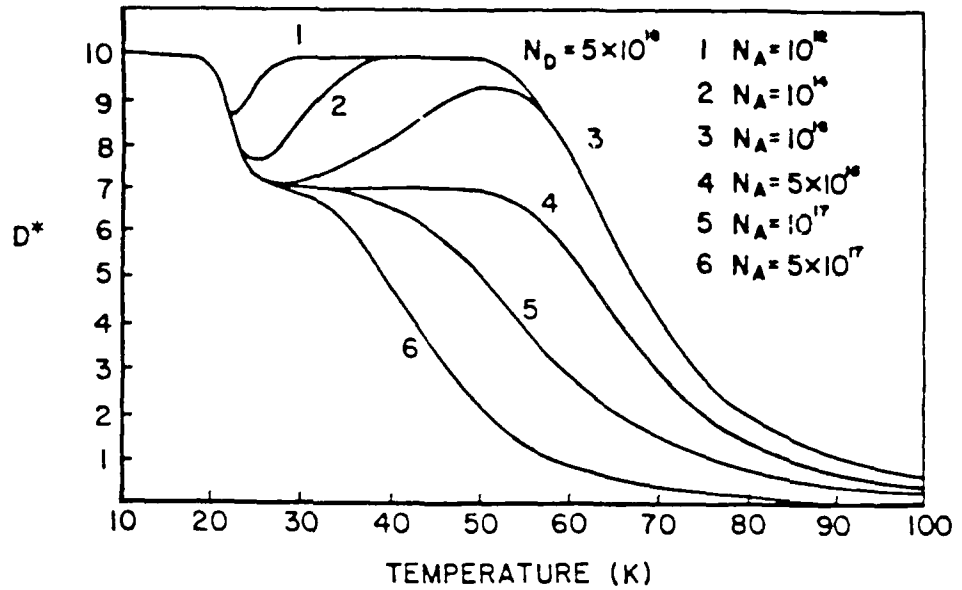


Figure 3. The detectivity (on a relative scale) of a model counterdoped system as a function of acceptor concentration and temperature for a fixed donor concentration and $B_D = 6 \times 10^{-10} / T^{1.5}$ (cm³/sec).

As the background flux is turned on optical absorption of valence electrons can proceed to the donor level only,



since the acceptor levels are already occupied by electrons. The valence hole is more likely to recombine at an ionized acceptor A^- ,



than at the neutral donor because of the widely different capture cross sections. Therefore, in Figure 3 for $T < 20K$ with the background flux on,

$$N_D^0 = N_D, \quad (28)$$

$$N_A^0 = N_A. \quad (29)$$

Under these conditions,

$$n_A = c_{A^+}/B_A \ll p \ll N_A, \quad N_A^- = n_A N_A / p, \quad (30)$$

$$n_D = c_{D^+}/B_D \gg p, \quad N_D^+ \gg p, \quad N_D^+ = N_D p / n_D, \quad (31)$$

and the charge neutrality equation is given by

$$p^2 [N_D / n_D + 1] = n_A N_A. \quad (32)$$

The solution for p becomes

$$p = (n_D n_A N_A / N_D)^{1/2} \sim \phi_B, \quad (33)$$

so that,

$$D^* \sim \phi_B^{-1/2}, \quad (34)$$

independent of temperature. This simply means that the detector is background limited before the onset of significant thermal hole generation.

The optical neutralization of acceptors and donors, Eqs. (28-29), and the lack of thermally generated carriers explain the flat portion of the D^* vs T curve for $T < 20K$. As the temperature is increased holes are thermally ionized from the boron acceptors to the valence band,



which contributes to the thermal g-r noise. Holes in the valence band may be recaptured at A^- centers, but then are rapidly thermally reemitted to the valence band. Therefore, a more likely process is the capture at the previously neutral donors



This process of hole capture by donors from acceptors mediated by the valence band lowers the detectivity because of the thermal rolloff owing to the thermal ionization of boron. At the same time, this process will be seen to improve the responsivity since the concentration of the D^+ principal IR-active level increases

Analytically, the region above $T > 20K$ is characterized by the following conditions,

$$a_A \ll p \ll N_A, \quad N_A^- = N_A a_A / p, \quad (37)$$

$$N_D \gg a_D \gg p, \quad N_D^+ = N_D p / a_D, \quad (38)$$

as before, except that now a_A possesses a significant thermal component. The solution for p is again given by

$$p = (a_D a_A N_A / N_D)^{1/2}, \quad (39)$$

and D^* is given by

$$D^* \sim [\tau_D / (B_D a_D) + \tau_A / (B_A a_A)]^{1/2}. \quad (40)$$

The two terms in Eq. (39) are of about the same order of magnitude for $20 < T < 25K$, except that a_A increases rapidly, owing to the thermal depopulation of the boron level, while a_D is relatively constant. This then provides the explanation for the thermal rolloff starting at $T = 20K$ in Figure 3.

The holes thermally emitted by the boron level experience different fates depending on the relative concentrations of boron with respect to donors. For $N_D \gg N_A$ the holes are quickly captured by the donors so that

$$N_A^- = N_A, \quad (41)$$

$$N_D^+ = N_A,$$

and the thermal rolloff in the detectivity is stopped. As can be seen in Figure curves 1, 2, and 3 tend back toward the background limited behavior.

For $N_A \gg N_D$ the transfer of holes from the boron level to the donor level is not complete at low temperatures. Therefore, a substantial density of neutral boron remains which contributes to the thermal noise. In particular, curves 5 and 6 in Figure 3 with $N_A > N_D$ exhibit lower detectivities for just that reason.

Of course, as the temperature is raised there is also a thermal depopulation of the donor level as well. The thermal rolloff due to the donors occurs at lower temperatures for higher boron concentrations, curve 6, than for $N_A = N_D$, curve 4. As the donor level gets rid of the holes some of the holes will be captured by the negatively ionized boron centers. Otherwise a large hole density exists in the valence band.

The cases depicted in Figure 3 exhibit comparable detectivities, but the corresponding responsivities vary by orders of magnitude. Several responsivity curves are shown in Figure 4. The best responsivities result for $N_A \geq N_D$. Undercompensating the donors results in lower responsivities. Overcompensation gives slightly higher responsivities, but at the price of lower detectivities and lower operating temperatures.

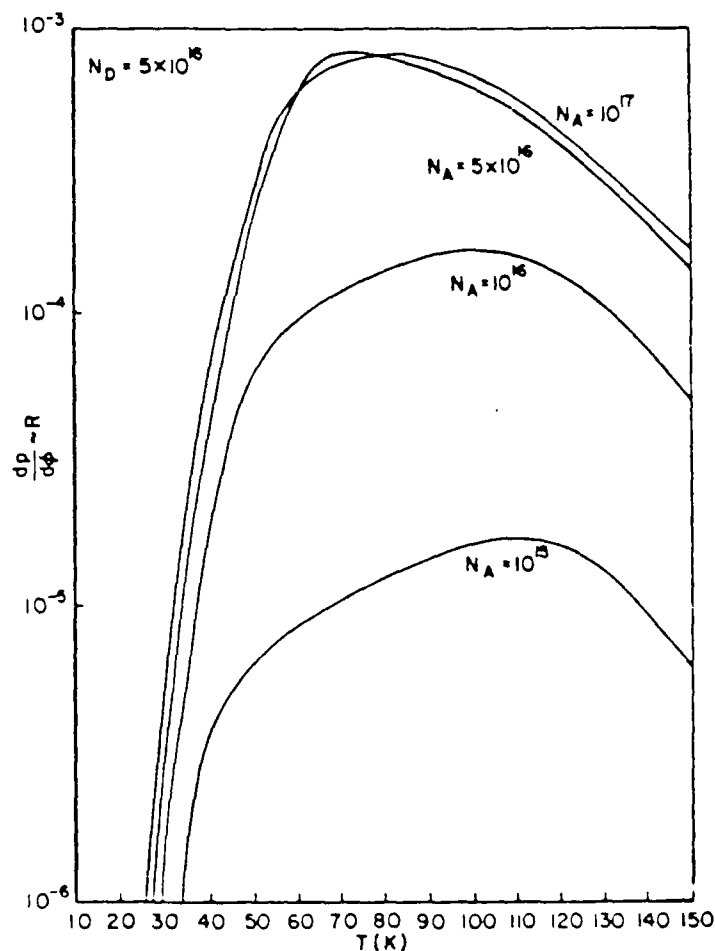


Figure 4. The responsivity (on a relative scale) for a model counterdoped system as a function of acceptor concentration and temperature for $B_D = 6 \times 10^{-10} / T^{1.5}$ (cm³/sec).

The behavior of responsivity in Figure 4 can be understood as follows. As the temperature is increased holes are thermally emitted from the boron level to the valence band and are subsequently captured at the neutral donors. This increases the density of D^+ centers which improves the quantum efficiency and

carrier lifetime. Increasing the temperature further results in thermal depopulation of the donor levels so that the quantum efficiency and lifetime decrease as does the responsivity.

The principal conclusions that emerge from this part of the parametric modeling effort are as follows. First, a dramatic improvement in the T_{BLIP} is realized for counterdoped systems over otherwise comparable conventionally doped systems. For the single-valent donor system the best responsivities and simultaneously best detectivities, with the the highest T_{BLIP} , are achieved for equal compensation of the donor concentration.

With these preliminary considerations out of the way, we may turn to a more realizable system⁵⁻⁷. This system consists of the positive divacancy level 0/+ at $E_D=200$ meV with the peak response at 4 μ m. The V_2^+ positive divacancies can be produced by e-beam irradiation of p-type silicon with the dose adjusted to match the density of acceptors. Proper annealing procedure must be followed to repair the lattice damage while maintaining a high density of the divacancies. I model this system using the parameters from Table 1, except as noted below. The peak photoabsorption cross section for the +/0 divacancy transition is estimated to be $4 \times 10^{-16} \text{ cm}^2$ by Humphreys et al⁸ and $2.5 \times 10^{-16} \text{ cm}^2$ by Brotherton et al⁹ which is consistent with the value in Table 1 adopted for the divacancy in the present work. For modeling purposes, I adopt $B_D = 6 \times 10^{-6} / T^{1.5} \text{ cm}^3/\text{sec}$, although the temperature dependence of the hole recombination coefficient at neutral divacancy is not known. The numerical constant has been adjusted to correspond to the measured recombination cross section in the 71-95K range of $4 \times 10^{-16} \text{ cm}^2$ obtained by Brotherton et al via DLTS. The donor activation energy is taken to be $E_D=200$ meV.

There is a choice of acceptors for the p-type dopant of the starting material: boron, aluminum, gallium, and indium. Figure 5 shows the detectivity and responsivity for these four choices of the starting p-type material. The responsivity for indium doping is too small to be displayed on the scale of the drawing. From the detectivity curves it appears that indium might be the preferred choice given its high thermal activation energy which delays its thermal rolloff to higher temperatures than for the other p-type dopants. The low value of the responsivity using indium doped silicon mitigates against this choice.

The problem with indium can be explained by the following argument. As explained earlier, responsivity increases with the increase in the D^+ concentration. D^+ are created by the hole capture from the valence band with the holes themselves thermally emitted by the acceptors. The deeper acceptors start emitting holes thermally at higher temperatures than does the shallow boron acceptor.

⁵Gross, C., Mattausch, R. J., and Viola, T. J., "Characteristics of infrared photodetectors produced by radiation doping," J. Appl. Phys. **44**, 735 (1973).

⁶Maher, E. F., Eddolls, D. V., Holeman, B. R., and Humphreys, R. G., "Electron-irradiated extrinsic silicon detectors for 3-5 μ m focal-plane arrays,"

⁷Electronics Letters **18**, 216 (1982).

⁸Humphreys, R. G., Webber, R. F., and Holeman, B. R., "An extrinsic Si thermal-imaging array," Infrared Physics **25**, 647 (1985).

⁹Humphreys, R. G., Brand, S., and Jaros, M., "Electronic structure of the divacancy in silicon," J. Phys. C**16**, 2337 (1983).

⁹Brotherton, S. D., Parker, G. J., and Gill, A., "Photoionization cross section of electron irradiation induced levels in silicon," J. Appl. Phys. **54**, 5112 (1982).

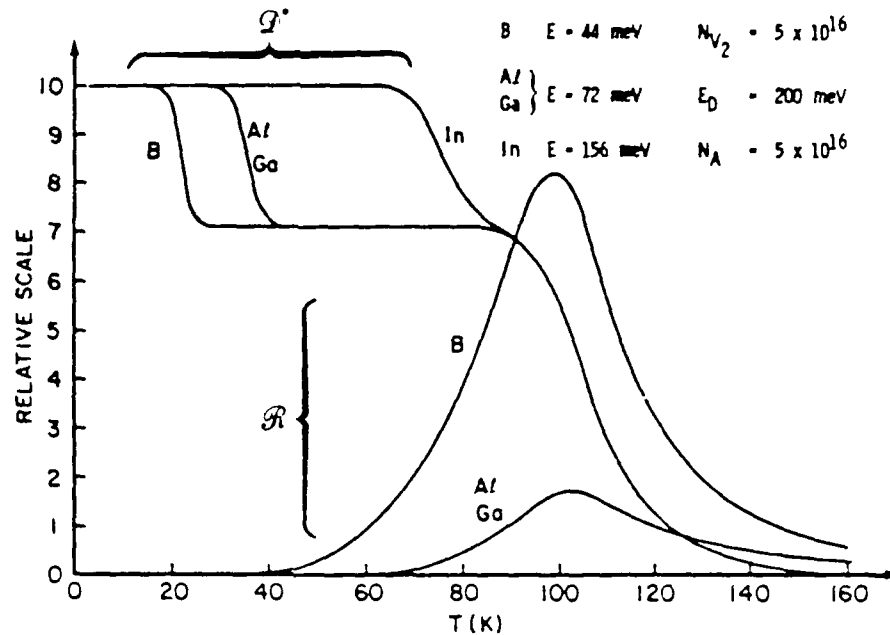


Figure 5. Detectivity and responsivity (on a relative scale) of a counterdoped detector with the divacancy deep donors as the principal IR-level and with four choices for the acceptor counterdopant: boron, aluminum, gallium, and indium.

In particular, at the temperature where there is a significant transfer of holes from indium to the divacancy, the divacancy itself begins to emit holes thermally back to the valence band. On the other hand, boron is well into the exhaustion region with all the holes captured by the divacancies before the divacancy caused thermal rolloff begins at about 90K. This is consistent with the T_{BLIP} of 100K, reported by Maher et al, for a similar background flux.

Figure 5 indicates that the best choice for the p-type starting material is that containing the shallowest acceptor. It is important that the knee of the D^* curve, which determines T_{BLIP} , is at the same temperature as the peak in the responsivity.

4.0 CONCLUSIONS

Before restating the main conclusions of this work, a few words are in order regarding the sensitivity of the results with respect to variations of the input parameters. The principal uncertainties concern the magnitudes and the temperature dependence of the recombination coefficients. These magnitudes affect T_{BLIP} , as seen in Figure 2. It is claimed here only that several orders of magnitude reduction in the recombination coefficient, which is expected physically for repulsive centers, will produce the dramatic effect on T_{BLIP} . The temperature dependence of the recombination coefficients mostly affects the shape and not the magnitude of the calculated curves. The main conclusions of this work are based on physical arguments regarding carrier dynamics and are largely insensitive to the numerical inputs.

The model employed in this work indicates large improvement in T_{BLIP} for the counterdoped system, on the order of tens of degrees. The best responsivities and detectivities are obtained for exact compensation of the deep donor, although the responsivities are not very sensitive to the variation of the compensation ratio around unity. It is recommended that the shallowest possible acceptor be used to compensate the deep donor in order to enhance the responsivity.

5.0 ACKNOWLEDGEMENTS

The author is indebted to Dr. Melvin C. Ohmer (AFWAL/MLPO, Wright-Patterson Air Force Base, OH) and Mr. John A. Detrio (University of Dayton Research Institute, Dayton, OH) for many useful discussions and for their encouragement.

AD-A231 413
WL-TR-91-4048



COUNTERDOPED HIGH TEMPERATURE, SILICON
ARRAY INFRARED DETECTOR

John A. Baker

Universal Energy Systems, Inc.
4401 Dayton-Xenia Road
Dayton, Ohio 45432

May 1991

Final Report for Period April 1986 - April 1987

Approved for public release; distribution is unlimited.

MATERIALS DIRECTORATE
WRIGHT LABORATORY
AIR FORCE SYSTEMS COMMAND
WRIGHT-PATTERSON AIR FORCE BASE, OHIO 45433-6533

23 JUN 1991

Unclassified

SECURITY CLASSIFICATION OF THIS PAGE

REPORT DOCUMENTATION PAGE				Form Approved OMB No. 0704-0188	
1a. REPORT SECURITY CLASSIFICATION Unclassified			1b. RESTRICTIVE MARKINGS		
2a. SECURITY CLASSIFICATION AUTHORITY			3. DISTRIBUTION/AVAILABILITY OF REPORT Approved for Public Release; Distribution is Unlimited		
2b. DECLASSIFICATION/DOWNGRADING SCHEDULE					
4. PERFORMING ORGANIZATION REPORT NUMBER(S)			5. MONITORING ORGANIZATION REPORT NUMBER(S) WL-IR-91-4048		
6a. NAME OF PERFORMING ORGANIZATION Universal Energy Systems, Inc.		6b. OFFICE SYMBOL (If applicable)	7a. NAME OF MONITORING ORGANIZATION Materials Directorate (WL/MLPU) Wright Laboratory		
6c. ADDRESS (City, State, and ZIP Code) 4401 Dayton-Xenia Rd Dayton OH 45432			7b. ADDRESS (City, State, and ZIP Code) Wright-Patterson AFB OH 45433-6533		
8a. NAME OF FUNDING/SPONSORING ORGANIZATION Materials Directorate		8b. OFFICE SYMBOL (If applicable) WL/MLPU	9. PROCUREMENT INSTRUMENT IDENTIFICATION NUMBER F33615-86-C-5091		
8c. ADDRESS (City, State, and ZIP Code) Wright Laboratory Wright-Patterson AFB OH 45433-6533			10. SOURCE OF FUNDING NUMBERS		
			PROGRAM ELEMENT NO. 65502F	PROJECT NO. 3005	TASK NO. 50
					WORK UNIT ACCESSION NO. 79
11. TITLE (Include Security Classification) Counterdoped High temperature, Silicon Array Infrared Detector					
12. PERSONAL AUTHOR(S) Baker, John A.					
13a. TYPE OF REPORT Final Report		13b. TIME COVERED FROM 4/86 TO 4/87		14. DATE OF REPORT (Year, Month, Day) May 1991	
15. PAGE COUNT 88					
16. SUPPLEMENTARY NOTATION					
17. COSATI CODES			18. SUBJECT TERMS (Continue on reverse if necessary and identify by block number)		
FIELD	GROUP	SUB-GROUP			
17	05		Counterdoping, silicon, electron irradiation, infrared detector, extrinsic		
19. ABSTRACT (Continue on reverse if necessary and identify by block number)					
A counterdoped infrared detector system consisting of a silicon substrate doped with boron and divacancies has been created.					
High purity polycrystalline silicon was further purified by float zoning to reduce the impurity levels still present; it was then back doped with boron. Electron irradiation was used to create the divacancies which become the active infrared centers. Boron served to compensate the newly created divacancies thus producing only positively charged divacancies; these positively charged divacancies are stable under illumination. The experimental results thus verify the theoretical model postulated by Elliott for counterdoping.					
A theoretical analysis of multivalent statistics as applied to counterdoped detectors has developed an extended model for counterdoped detectors. This model has identified the relevant parameters which control the operating temperature and figure of merit for the					
20. DISTRIBUTION/AVAILABILITY OF ABSTRACT <input type="checkbox"/> UNCLASSIFIED/UNLIMITED <input type="checkbox"/> SAME AS RPT <input checked="" type="checkbox"/> DTIC USERS			21. ABSTRACT SECURITY CLASSIFICATION Unclassified		
22a. NAME OF RESPONSIBLE INDIVIDUAL Gail J. Brown			22b. TELEPHONE (Include Area Code) (513) 255-4474		22c. OFFICE SYMBOL WL/MLPO

Block 19.

counterdoped detector. The model may be used to optimize doping concentration for the highest background limited infrared photoconductor (BLIP) operating temperature.

**END
FILMED**

DATE: 4-91

DTIC